

---

# Generating Safe Trajectories in Stochastic Dynamic Environments by Leveraging Information About Obstacle Motion

---



University of  
St Andrews

CS4099: MAJOR SOFTWARE PROJECT

*Author:* Alexander WALLAR      *Supervisor:* Dr. Michael WEIR

April 10, 2015

## **Abstract**

---

## Declaration

---

I declare that the material submitted for assessment is my own work except where credit is explicitly given to others by citation or acknowledgement. This work was performed during the current academic year except where otherwise stated.

The main text of this project report is NNN words long, including project specification and plan.

In submitting this project report to the University of St Andrews, I give permission for it to be made available for use in accordance with the regulations of the University Library. I also give permission for the title and abstract to be published and for copies of the report to be made and supplied at cost to any bona fide library or research worker, and to be made available on the World Wide Web. I retain the copyright in this work.

---

## Acknowledgements

---

The author would like to thank Dr. Michael Weir and Dr. Erion Plaku for their valuable insight throughout the development of this project and the School of Computer Science for a truly phenomenal undergraduate education. The author would like to credit the most honourable Aleksejs Sazonovs for providing the L<sup>A</sup>T<sub>E</sub>X template used in this report. The author would like to show his great appreciation to the open source robotics community for providing countless free online resources and software such as ROS and RViz used throughout this project. The author would also like to thank his wife, Jessica, for putting up with the late nights and limited contact whilst this project slowly enveloped his life.

---

## Contents

---

<b>1</b>	<b>Introduction</b>	<b>11</b>
<b>2</b>	<b>Context Survey</b>	<b>13</b>
2.1	Evolutionary Algorithms . . . . .	13
2.2	Safe Interval Path Planning . . . . .	14
2.3	Sampling in Space-time . . . . .	14
2.4	Probabilistic Methods . . . . .	14
2.5	Limitations of Related Work . . . . .	15
<b>3</b>	<b>Software Development Framework</b>	<b>16</b>
3.1	Development Methodology . . . . .	16
3.2	Source Control . . . . .	16
<b>4</b>	<b>Objectives</b>	<b>17</b>
4.1	Primary . . . . .	17
4.2	Secondary . . . . .	17
<b>5</b>	<b>Design</b>	<b>18</b>
5.1	Space-time Bug Algorithm . . . . .	18
5.2	Potential Fields . . . . .	19
5.3	Space-time Roadmap . . . . .	20
5.4	Probabilistic Roadmap With Best First Search . . . . .	21

## CONTENTS

---

<b>6 Planner Methodology</b>	<b>22</b>
6.1 Dynamic Obstacles . . . . .	22
6.1.1 Definition . . . . .	22
6.1.2 Cost Distribution . . . . .	23
6.1.3 Equations of Motion . . . . .	24
6.1.4 Available Information . . . . .	25
6.2 Planning Algorithm . . . . .	25
6.2.1 Building the Roadmap . . . . .	25
6.2.2 Searching the Graph . . . . .	26
6.2.3 Replanning . . . . .	31
6.2.4 Discussion . . . . .	31
<b>7 Implementation</b>	<b>33</b>
7.1 Initial . . . . .	33
7.2 Final . . . . .	33
<b>8 Experimental Setup</b>	<b>35</b>
8.1 Design . . . . .	35
8.2 Metrics . . . . .	36
8.2.1 Safety . . . . .	36
8.2.2 Computational Time . . . . .	37
8.2.3 Variance . . . . .	37
8.3 Scenes . . . . .	37
<b>9 Results</b>	<b>41</b>
9.1 Safety . . . . .	41
9.1.1 Variance . . . . .	42
9.2 Computational Time . . . . .	44
9.2.1 Variance . . . . .	45
9.3 Behaviour . . . . .	46
<b>10 Discussion</b>	<b>49</b>
10.1 Future Work . . . . .	49
10.1.1 Pruning the Search Tree . . . . .	49

## CONTENTS

---

10.1.2 Variable Speed and Wait Time . . . . .	49
10.1.3 Increasing Robot Dimensionality . . . . .	50
10.1.4 Real World Experiments . . . . .	50
10.1.5 More Complex Models of Obstacle Behaviour . . . . .	50
10.1.6 Multi-robot Coordination . . . . .	51
10.2 Evaluation & Conclusion . . . . .	51
<b>11 Ethics</b>	<b>52</b>

---

## List of Figures

---

5.1	This image shows an example of the bug algorithm determining hit points obstacles in order to move around them to reach the goal. This image is courtesy of Dr. Erion Plaku.	19
6.1	A plot depicting the three dimensional normal distribution $\mathcal{N}(\cdot)$ that is used as a basis function for the obstacle cost distribution. The more red an area, the higher the cost. The more blue an area, the lower the cost. . . . .	23
6.2	Cost distributions indicating the likelihood that a dynamic obstacle will be at a certain location within a given time interval. These figures show how this distribution changes over time. The sequence progress from left to right, top to bottom . . . . .	24
6.3	An example of a probabilistic roadmap generated in free space without the presence of obstacles. The nodes are represented by the circles and the red line as the edges between the nodes. . . . .	27
6.4	A depiction of the search tree generation for a given probabilistic roadmap. The $x$ and $y$ axes represent the $x$ and $y$ location of the node, and the vertical axis represents time. The sequence progress from left to right, up to down. The final image in sequence also shows the path taken by the robot in red. . . . .	29
6.5	A sequence of images showing the progression of the cost distribution for the set of dynamic obstacles over time used for the search tree shown in Fig. 6.4. The sequence progresses from left to right, up to down. . . . .	30
7.1	A diagram depicting the work flow for the implementation. The Dodger library can either generate a path and export to a JSON file which can then be visualized in Matplotlib or RViz using one of the Python scripts provided or user code can read the exported JSON to control robots or visualize the paths. The library can also be imported by user code to either visualize paths or control a robot with ROS. . . . .	34
8.1	A depiction of how the dynamic obstacles progress over time for Scene 1. No noise is added to their trajectories in order to display the pure velocity function used for their motion. The sequences progresses from left to right, top to bottom. . . . .	38

## LIST OF FIGURES

---

8.2	A depiction of how the dynamic obstacles progress over time for Scene 2. No noise is added to their trajectories in order to display the pure velocity function used for their motion. The sequences progresses from left to right, top to bottom. . . . .	39
8.3	A depiction of how the dynamic obstacles progress over time for Scene 3. No noise is added to their trajectories in order to display the pure velocity function used for their motion. The sequences progresses from left to right, top to bottom. . . . .	40
9.1	Plots showing how the minimum distance to any obstacle for a path changes as the speed increases for various amounts of obstacle position uncertainties. The horizontal axis represents the speed of the robot and the vertical axis represents the minimum distance to obstacles along the path. The different lines on each plot represent experiments with differing amounts of noise and the error bars represent one standard deviation. On the left is the graph for Dodger and on the right is the graph for the potential fields planner. . . . .	42
9.2	Plots showing how the maximum cost for a path changes as the speed increases for various amounts of obstacle position uncertainties. The horizontal axis represents the speed of the robot and the vertical axis represents the maximum cost along the path. The different lines on each plot represent experiments with differing amounts of noise and the error bars represent one standard deviation. On the left is the graph for Dodger and on the right is the graph for the potential fields planner. . . . .	43
9.3	Plots showing how the average cost for a path changes as the speed increases for various amounts of obstacle position uncertainties. The horizontal axis represents the speed of the robot and the vertical axis represents the average cost along the path. The different lines on each plot represent experiments with differing amounts of noise and the error bars represent one standard deviation. On the left is the graph for Dodger and on the right is the graph for the potential fields planner. . . . .	43
9.4	Plots showing how the standard deviation for the minimum distance along a path changes as the noise injected into the obstacle trajectories increases. The horizontal axis represents the amount of noise and the vertical axis represents the standard deviation. The different lines indicate different speeds that the robot was travelling. On the left is the graph for Dodger and on the right is the graph for the potential fields planner. . . . .	44
9.5	Plots showing how the standard deviation for the maximum cost and average cost along a path changes as the noise injected into the obstacle trajectories increases. The horizontal axis represents the amount of noise and the vertical axis represents the standard deviation. The different lines indicate different speeds that the robot was travelling. On the left is the graph for Dodger and on the right is the graph for the potential fields planner. The top row is for the maximum cost and the bottom row is the for the average cost. . . . .	44
9.6	Plots showing how the computational to generate a path changes as the speed increases for various amounts of obstacle position uncertainties. The horizontal axis represents the speed of the robot and the vertical axis represents the computational time to generate the path. The different lines on each plot represent experiments with differing amounts of noise and the error bars represent one standard deviation. On the left is the graph for Dodger and on the right is the graph for the potential fields planner. . . . .	45
9.7	Plots showing how the standard deviation for the computational cost to generate a path changes as the noise injected into the obstacle trajectories increases. The horizontal axis represents the amount of noise and the vertical axis represents the standard deviation. The different lines indicate different speeds that the robot was travelling. On the left is the graph for Dodger and on the right is the graph for the potential fields planner. . . . .	46

## LIST OF FIGURES

---

9.8 Images showing the progression of the robot, represented by the quadrotor, following a path generated by Dodger through Scene 1 from the initial configuration, represented by the red quadrotor shape, to the goal configuration, the green quadrotor shape. The obstacles are represented by the mobile ground robots and the path of the robot is shown by the blue line. The sequence of images progress from left to right, up to down. . . . .	47
9.9 Images showing the progression of the robot, represented by the quadrotor, following a path generated by the potential fields planner through Scene 1 from the initial configuration, represented by the red quadrotor shape, to the goal configuration, the green quadrotor shape. The obstacles are represented by the mobile ground robots and the path of the robot is shown by the blue line. The sequence of images progress from left to right, up to down. . . . .	48
11.1 A picture of a possible vessel for the robot uprising . . . . .	52
11.2 Plots showing how the minimum distance to any obstacle for a path changes as the speed increases for various amounts of obstacle position uncertainties. The horizontal axis represents the speed of the robot and the vertical axis represents the minimum distance to obstacles along the path. The different lines on each plot represent experiments with differing amounts of noise and the error bars represent one standard deviation. . . . .	54
11.3 Plots showing how the maximum cost for a path changes as the speed increases for various amounts of obstacle position uncertainties. The horizontal axis represents the speed of the robot and the vertical axis represents the maximum cost along the path. The different lines on each plot represent experiments with differing amounts of noise and the error bars represent one standard deviation. . . . .	55
11.4 Plots showing how the average cost for a path changes as the speed increases for various amounts of obstacle position uncertainties. The horizontal axis represents the speed of the robot and the vertical axis represents the average cost along the path. The different lines on each plot represent experiments with differing amounts of noise and the error bars represent one standard deviation. . . . .	55
11.5 Plots showing how the standard deviation for the minimum distance along a path changes as the noise injected into the obstacle trajectories increases. The horizontal axis represents the amount of noise and the vertical axis represents the standard deviation. The different lines indicate different speeds that the robot was travelling. . . . .	56
11.6 Plots showing how the standard deviation for the maximum cost and average cost along a path changes as the noise injected into the obstacle trajectories increases. The horizontal axis represents the amount of noise and the vertical axis represents the standard deviation. The different lines indicate different speeds that the robot was travelling. On the left is the graph for Dodger and on the right is the graph for the potential fields planner. . . . .	56
11.7 Plots showing how the computational time to generate a path changes as the speed increases for various amounts of obstacle position uncertainties. The horizontal axis represents the speed of the robot and the vertical axis represents the computational time to generate the path. The different lines on each plot represent experiments with differing amounts of noise and the error bars represent one standard deviation. . . . .	57
11.8 Plots showing how the standard deviation for the computational cost to generate a path changes as the noise injected into the obstacle trajectories increases. The horizontal axis represents the amount of noise and the vertical axis represents the standard deviation. The different lines indicate different speeds that the robot was travelling. . . . .	57

---

## LIST OF FIGURES

11.9 Plots showing how the minimum distance to any obstacle for a path changes as the speed increases for various amounts of obstacle position uncertainties. The horizontal axis represents the speed of the robot and the vertical axis represents the minimum distance to obstacles along the path. The different lines on each plot represent experiments with differing amounts of noise and the error bars represent one standard deviation. On the left is the graph for Dodger and on the right is the graph for the potential fields planner. . . . .	58
11.10Plots showing how the maximum cost for a path changes as the speed increases for various amounts of obstacle position uncertainties. The horizontal axis represents the speed of the robot and the vertical axis represents the maximum cost along the path. The different lines on each plot represent experiments with differing amounts of noise and the error bars represent one standard deviation. On the left is the graph for Dodger and on the right is the graph for the potential fields planner. . . . .	59
11.11Plots showing how the average cost for a path changes as the speed increases for various amounts of obstacle position uncertainties. The horizontal axis represents the speed of the robot and the vertical axis represents the average cost along the path. The different lines on each plot represent experiments with differing amounts of noise and the error bars represent one standard deviation. On the left is the graph for Dodger and on the right is the graph for the potential fields planner. . . . .	59
11.12Plots showing how the standard deviation for the minimum distance along a path changes as the noise injected into the obstacle trajectories increases. The horizontal axis represents the amount of noise and the vertical axis represents the standard deviation. The different lines indicate different speeds that the robot was travelling. On the left is the graph for Dodger and on the right is the graph for the potential fields planner. . . . .	60
11.13Plots showing how the standard deviation for the maximum cost and average cost along a path changes as the noise injected into the obstacle trajectories increases. The horizontal axis represents the amount of noise and the vertical axis represents the standard deviation. The different lines indicate different speeds that the robot was travelling. On the left is the graph for Dodger and on the right is the graph for the potential fields planner. The top row is for the maximum cost and the bottom row is the for the average cost. . . . .	60
11.14Plots showing how the computational to generate a path changes as the speed increases for various amounts of obstacle position uncertainties. The horizontal axis represents the speed of the robot and the vertical axis represents the computational time to generate the path. The different lines on each plot represent experiments with differing amounts of noise and the error bars represent one standard deviation. On the left is the graph for Dodger and on the right is the graph for the potential fields planner. . . . .	61
11.15Plots showing how the standard deviation for the computational cost to generate a path changes as the noise injected into the obstacle trajectories increases. The horizontal axis represents the amount of noise and the vertical axis represents the standard deviation. The different lines indicate different speeds that the robot was travelling. On the left is the graph for Dodger and on the right is the graph for the potential fields planner. . . . .	61

---

## Notation

---

Notation	Description
$a$	A dynamic obstacle
$A$	Set of dynamic obstacles
$P_a(\cdot)$	Cost distribution for a single dynamic obstacle, $a$
$P(\cdot)$	Cost distribution for a set of dynamic obstacles
$\mathcal{N}(\cdot)$	Three dimensional normal distribution
$\dot{\zeta}(\cdot)$	Velocity function for a dynamic obstacle
$\zeta(\cdot)$	Predicted trajectory of a dynamic obstacle
$\tilde{\zeta}(\cdot)$	Observed trajectory for a dynamic obstacle
$C(\cdot)$	Dynamic edge cost for the probabilistic roadmap excluding revisiting penalty
$TC(\cdot)$	Dynamic edge cost for the probabilistic roadmap including revisiting penalty
$I$	Initial configuration of a dynamic obstacle
$\epsilon$	Amount of noise injected into a dynamic obstacle's trajectory
$\xi$	Last configuration used for trajectory prediction
$T$	Last time used for trajectory prediction
$\alpha$	Multiplicative weight for the variance in $\mathcal{N}(\cdot)$
$\beta$	Additive weight for the variance in $\mathcal{N}(\cdot)$
$\gamma$	Exponential constant used for weighting basis functions in $P$
$\psi$	Multiplicative weight for the cost distribution in $TC$
$\omega$	Multiplicative weight for revisiting a node in $TC$

# CHAPTER 1

---

## Introduction

---

Path planning is a very important problem in robotics and computer science. It is the problem of generating a path through an environment that if followed by a robot, would move the robot from some initial configuration to a goal configuration without coming into collision with any obstacles on the way. This problem may seem easy for a human to solve, just walk around the obstacles and get to the goal, but for a robot it can be extremely difficult. As humans, we have amazing perception abilities and an unparalleled ability to assess the risk we perceive and plan around it. These capabilities are not as developed in artificial intelligence. Humans can walk around environments which are dynamic and uncertain and (usually) reach wherever they are going without running into moving obstacles or hitting walls. This is because as humans, we can determine automatically where things are going to be in the future by looking at their past locations and use this information to build safe, collision free paths to our goals. Imagine you are driving a car and reach an intersection, you stop because you see a car coming from the right. You have a choice to either move forward crossing over the future path of the other car, or to wait for the car to pass. By judging how far the car is away from you and how fast it is moving, you can automatically determine whether or not it is safe to cross the road. Likewise, imagine you are a waiter in a busy, hectic restaurant. You have to bring an order to hungry customers. You are able to bring the customers the food by predicting where other waiters and customers are going to be whilst you move through environment in order to avoid spilling the food and sacrificing your tip. Our brains do this planning and prediction automatically in order to generate safe paths through stochastic dynamic environments. The aim of this project is to use given information about the future motion of obstacles by an external system in order to generate safer paths than state of the art planners that have been designed for and operate in dynamic environments.

There has been outstanding progress by the robotics community to develop algorithms that are able to plan the motion of a robot in order for it to reach its goal. From this community, three different paradigms for path generation and motion planning have emerged, geometric algorithms, reactive algorithms, and sampling based approaches [1, 2]. Geometric algorithms such as the bug algorithm [3] or visibility graph algorithm [4], use the geometry of the environment to create exact geometric paths to the goal. These algorithms almost always have no random component, and for a given environment, will return the same path every time. The second paradigm for motion planning, reactive algorithms, move the robot to the next best location at the current time for a given sensing radius. These approaches are vastly dominated by the use of potential fields in order to determine the direction that a robot should move. The approaches use a combination of an attractive potential function to guide the robot towards a goal and a repulsive potential function that keeps the robot from coming into contact with obstacles. The robot moves forward in time by determining the direction it should move that would minimize the combined potentials. Sampling based approaches approximately discretize the environment, also known

as the search space, in order to describe its connectivity by sampling plausible configurations and how to move between them. With the discretization, usually in the form of a graph or a tree, paths to the goal are extracted using shortest path algorithms which seek to minimize a given objective function. These approaches are becoming exceedingly popular due to their running time and how they are able to scale for high dimensional systems.

This project aims to utilize developments in motion planning, particularly sampling based motion planning in order to move a robot safely from an initial configuration to a goal configuration in a stochastic dynamic environment by leveraging information about the trajectories of dynamic obstacles. By having some idea about where the obstacles are going to move in the future, it is possible to use sampling based techniques that can sample collision free and low risk paths to the goal in space-time. The goal of this project is to create algorithms that can provide low cost paths to the goal by utilizing the information available about how the obstacles in an environment will move. This work introduces a novel representation of dynamic obstacles and a novel algorithm for searching the environment in space-time. Proofs are also provided that can guarantee the completeness of the search such that the algorithms will always provide a path to the goal. This problem is important because if robots are interacting with humans, the robot must move safely in order not to come into contact with and hurt humans as well as minimize the damage that can possibly occur to itself. Likewise, imagine a situation where a robot is deployed to an environment for a long period of time. By generating safe paths (i.e. paths that have an insignificant chance of colliding with an obstacle), the robot can be deployed for longer periods of time without maintenance, because it would be less likely that it would get damaged as a result of a collision. A solution to this problem can provide safer paths for the operating environment and the robot by leveraging information that can be extracted about where obstacles are moving. Likewise, this problem is important because there exists systems that are able to predict the motions of obstacles, however there is a lack of systems that use this knowledge to generate safe paths.

# CHAPTER 2

---

## Context Survey

---

For years the planning community has been developing algorithms that allow robots to navigate through environments to reach a goal. As research progressed, so did the complexity of the environments that the robots needed to move through. It started with static obstacles which remain stationary for the entirety of the plan, then on to dynamic obstacles with stochastic motion, to dynamic obstacles that have predictable paths that planners can exploit. For the last situation, a number of planners implementing different techniques have been created. Techniques include evolutionary computation on geometric structures in space-time to generate paths, safe interval path planning, sampling based space-time search using collision prediction, and probabilistic methods. Note that this context survey only covers approaches that make use of models of obstacle behaviour and discards approaches that purely react to obstacle motion.

### 2.1 Evolutionary Algorithms

Wang et al. used a genetic algorithm [5] that would generate a path around the static and dynamic obstacles [6]. The obstacles were encoded by a set of vertices in a polygon. The chromosomes used in the genetic algorithms represented the paths that the robot can take to move to the goal where the path is comprised of the initial and goal points along with obstacle vertices. The path generated for the robot would cling to the perimeter of an obstacle, until it could move towards the goal similar to the bug algorithm [3]. The time at which the robot would reach each node was also encoded into the path. Moving obstacles were represented as static obstacles for a given time. Upon a sensed change in the environment such as a dynamic obstacle veering off its prescribed trajectory, replanning using the genetic algorithm was used to regenerate a collision free path.

Smierzchalski and Michalewicz have also used an evolutionary approach [7] where the chromosome represents the spatio temporal path in order to plan the movements of a ship in a harbour where the obstacles are other ships in a shipping lane [8]. The higher the evaluation for the chromosome (i.e. the path) the safer and shorter the path is. Unlike the work done by Wang et al. the path can be comprised of any point in the search space. The obstacles were represented geometrically and the dynamic obstacles were represented by their initial configuration and velocity. Since the path represented in a spatio-temporal fashion, the genetic algorithm is able to determine if a path will collide with a dynamic obstacle by deducing where the dynamic obstacle will be at each time step along the path and checking for a collision. Replanning using the evolutionary algorithm was implemented to account for obstacles deviating from their prescribed trajectories.

Dunwei and Na used particle swarm optimization (PSO) [9] to generate local paths around dynamic obstacles that are represented by trajectory bands [10]. In order to account for the stochasticity in the obstacle trajectories, a distance around each obstacle's trajectory was used to describe how much the obstacle can deviate from it. Using these bands, an objective function was created that represents the safety of the generated path. PSO was used to generate a path that could minimize the objective function.

## 2.2 Safe Interval Path Planning

Narayanan et al. and Phillips et al. have developed algorithms for generating safe paths to guide a robot to a goal configuration by determining time intervals for which it would be safe to travel through certain areas in the search space and using a graph search algorithm to find a path to the goal that only intersects safe time intervals [11, 12]. Safe time intervals are determined by iterating through the trajectory of each obstacle and updating a query structure that can be used to check whether a certain space will be free for a given period of time. A lattice structure is used to discretize the search space and an A\* variant, Anytime Repairing A\* (ARA\*) [13] is used to search this lattice. This algorithm relies on the robot waiting at certain locations for areas to become free of obstacles before it is able move towards the goal.

## 2.3 Sampling in Space-time

Berg et al. have developed a sampling based approach that generates a probabilistic roadmap of the same dimension as the configuration space of the robot with time that takes into account static and dynamic obstacles. [14]. A novel graph search technique similar to D\* Lite [15] was implemented that can automatically repair the path when new information about obstacle motion is available such that the robot will not be led into a collision with an obstacle. Obstacles are represented by elongated objects in space-time and their stochasticity is represented by their size as the time away from the current time increases.

Hsu et al. have also created an algorithm that generates a probabilistic roadmap in space-time where each node represents the configuration of the robot and a time at which the robot would be at the configuration [16]. Using the probabilistic roadmap, a shortest path algorithm is used to find the fastest route from the initial configuration of the robot to the goal configuration. Obstacles are represented in a similar fashion as the work done by Berg et al. [14] except there is no representation of stochasticity. The planner handles updated information about the dynamic obstacles by updating the probabilistic roadmap and researching the graph for a path to the goal.

## 2.4 Probabilistic Methods

Jensen et al. developed an algorithm that uses a probabilistic obstacle model to represent and employs a gradient decent method to find a path to the goal [17]. A gradient decent approach tries to minimize the probability of the robot coming into collision with an obstacle along the path. This method is general but assumes that the robot has a sensing radius and is able to move in the direction that has the lowest probability of collision. Likewise, the paper shows that the combined probability model for the obstacles in the scene only has one global minima. The algorithm can also be adapted so that there is a trade off between the probability of collision and the length of the path.

Rodriguez et al. uses a dynamic probabilistic roadmap to find a global path to the goal and local kinodynamic motion planning to evade dynamic obstacles [18]. A self-repairing probabilistic roadmap is generated that takes into account the location of static obstacles. Using this roadmap, a global path to the goal is found using a graph search technique. The global path represents a sequence of sub-goal regions and a kinodynamic local planner using an approach similar to RRT [19] determines the local path that moves the robot to each sub-goal region in sequence. This approach allows obstacles which have been assumed to be stationary to move or have uncertainty in their positions. The probabilistic roadmap

will automatically repair itself upon obtaining updated information about the static obstacles such that no edge is in collision with an obstacle.

## 2.5 Limitations of Related Work

The main limitation of the developments described is that there is no solution that uses the obstacles' known stochastic trajectories to build probabilistic representations and use these representations to build complete low cost paths. Some of the algorithms currently either assume that the planner only knows that the obstacles will move randomly around a point [18] or that the obstacles will move along a fixed trajectory [16], and if they deviate, a new plan is developed. Hsu et al. assumed perfect information about the obstacle trajectories to build an initial path through the environment, and if the information was incorrect or the obstacles deviate from their prescribed trajectories, the planner develops a new route to the goal. Berg et al. increased the size of the dynamic obstacles in space time to account for random motion, but to plan around them, represented the obstacles as static objects in space-time thus not devising a cost metric for their motion. Likewise, the approaches that used safe interval path planning [11, 12], did not build probabilistic models of the obstacles, but instead determined intervals at which it would be safe to travel through certain areas and is thus heavily reliant on the robot waiting at certain locations. The evolutionary approaches described were geometric and also did account for the stochasticity in the known trajectories of the dynamic obstacles. The one approach that did create probabilistic models of the dynamic obstacles [17] employed a gradient decent method similar to that of potential fields that is described in Sec. 5.2 to be ineffective in certain situations and that a sampling based approach is more complete. All of these approaches lack an elegant, sampling based algorithm that can take into account the stochastic trajectories of dynamic obstacles in order to rely less heavily on replanning, and to make use of the available information from the environment. The approach described in this work develops a formal representation dynamic obstacles that is able to take into account their stochasticity and presents a novel sampling based approach that is able to generate low cost paths that can lead a robot to its goal.

# CHAPTER 3

---

## Software Development Framework

---

### 3.1 Development Methodology

Since this project is primarily research, an agile development methodology was used. There were no set requirements for the project, and instead the author was encouraged to produce results towards a goal. The solution was devised by determining a set of intermittent goals and possible solutions. As you can see in Ch. 5, four different solutions were designed and three were implemented, each using a different approach to solve the problem at hand. The development feedback loop worked by first listing the objectives and goals for the project, i.e. generating safe paths through dynamic environments. Once an algorithm was designed that the author was confident could solve this problem, it was implemented and tested both quantitatively and qualitatively. If the behaviour of the robot did not resemble the desired behaviour, the solution was either augmented to possibly change the behaviour of the robot, or a new solution was devised.

### 3.2 Source Control

As a method of storing and updating the codebase, source control was used. In particular, GitHub was used to store the code, its revisions, releases, and notes. Along with the main codebase, GitHub was used to store the scripts created for running tests and experiments and kept track of the experimental results during development. Only working and compilable code was pushed to the Git repository and since there was only one developer, a continuous integration server was not used. Instead, before a commit could be pushed to the server, the code had to be compilable and pass a set of sanity checks. These sanity checks consisted of checking whether roadmaps could still be generated and if the basic operations on the data structures still functioned properly.

# CHAPTER 4

---

## Objectives

---

### 4.1 Primary

The main objective of this work is to develop an algorithm that generates a quantitatively safe trajectory for a robot through an uncertain dynamic environment by utilizing information about how dynamic obstacles are going to move in the future and to develop a formal probabilistic representation of stochastic dynamic obstacles. This can be simply stated as determining the curvature that minimizes the line integral over the dynamic cost distribution for a given set of dynamic obstacles.

$$J(C, A) = \int_C \exp(P(x, y, t_0, t_m, A) + 1) ds \quad (4.1)$$

Eq. 4.1 describes the objective function,  $J$ , that needs to be minimized with respect to the curvature in order to determine the safest path through the environment. In Eq. 4.1, the function  $P$  is the cost surface for a given time interval and set of obstacles and represents the cost of coming in collision with or moving towards the trajectory of any obstacle in the environment. More description about  $P$  is given in Sec. 6.1.2 and is formally defined in Eq. 6.2. More precisely, the objective of this work to develop an algorithm that will provide an approximate solution to Eq. 4.2 which will return a significantly low cost path through a environment for a given set of obstacles. The solution is described in Sec. 6.2

$$\Gamma(A) = \arg \min_C J(C, A) \quad (4.2)$$

### 4.2 Secondary

The main secondary objective for this work is to show that the proposed solution can provide safer paths than standard planners such as potential fields by leveraging information about how the obstacles move through the environment. Quantitative and qualitative experiments have been conducted that provide evidence that the proposed solution does indeed produce safer paths based on the safety metrics that have been devised for this work. These results are shown in Ch. 9.

# CHAPTER 5

---

## Design

---

As with any research project, many different attempts were made to come up with a solution to the objectives stated in Ch. 4. Three different techniques were developed in sequence and one technique was theorized but never implemented to try and provide a solution that best matched the sought behaviour for the planner. The theorized technique included using a bug algorithm [3] in space-time to find a path through the dynamic environment. The first attempt was a simple potential field that would take into account the predicted trajectories of the obstacles, and leverage this information to provide safer paths. The second attempt included generating a probabilistic roadmap in relative space-time and using stock graph search algorithms such as Dijkstra's algorithm and Edmonds' algorithm to derive low costs paths through the environment. The last attempt, and the most successful is a planner that uses a two dimensional probabilistic roadmap to sample the search space and then uses Best First Search to expand nodes in space-time to determine the minimum cost path through the dynamic environment. These four attempts are described individually and in more detail in this section.

### 5.1 Space-time Bug Algorithm

The initial design for the algorithm was to use a bug algorithm that operates in space-time. Bug algorithms work by moving the robot towards the goal until it reaches an obstacle. Once an obstacle has been reached, the bug algorithm will move the robot along the edge of the obstacle until the obstacle is no longer between the robot and the goal. The robot will then move to the goal and repeat this process if necessary. An example of this algorithm in practice is shown in Fig. 5.1. This proposed design was going to treat the dynamic obstacles moving in two dimensions as three dimensional static obstacles in three dimensions where time is the third dimension. The robot would use the bug algorithm to move through the environment in three dimensions. A constraint would have been added to the movement of the robot which would be that it could not move backward in the last dimension, time. The benefit of this design is that completeness could be proven geometrically, it is a computationally simple algorithm, and it could be easily implemented for use on a mobile robot. This design was not implemented because of several fundamental flaws discovered during the design phase. Firstly, by thinking of dynamic obstacles as static obstacles in space-time, the robot would have to rely on perfect information about the movement of the dynamic obstacles, i.e. there could be very little uncertainty about the movements or predictions of the movements in the dynamic obstacles. For the planner to be able to handle uncertainty in the motion of the obstacles *a priori*, obstacles would need to be increased in their size (emphasizing the possible positions of the dynamic obstacles) as time increases. This could lead to possibly unrecoverable configurations because obstacles in space-time could be seen as overlapping thus not providing a collision

free area for the robot to move through. It was ultimately decided not to continue with this design but instead to leverage a more stochastic and probabilistic definition of the dynamic obstacles and to use planning techniques more suited for stochastic dynamic environments.

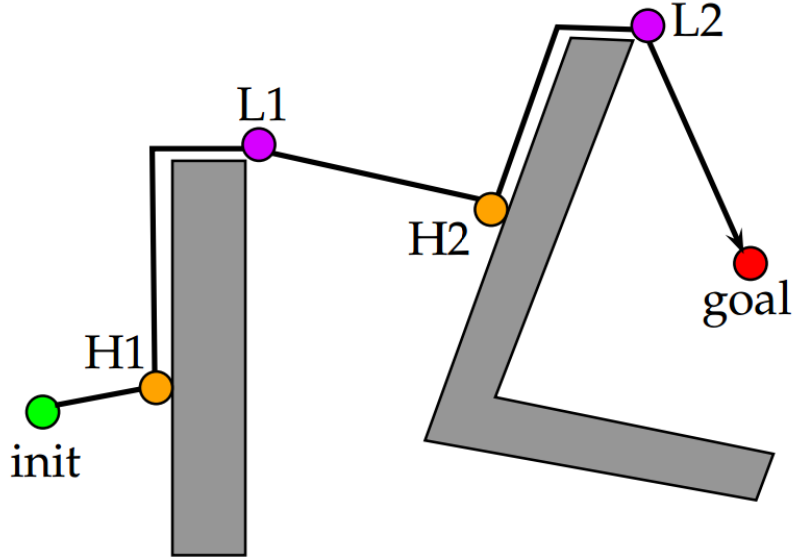


Figure 5.1: This image shows an example of the bug algorithm determining hit points obstacles in order to move around them to reach the goal. This image is courtesy of Dr. Erion Plaku.

## 5.2 Potential Fields

Using potential fields was an initial attempt to plan through uncertain dynamic environments since they are frequently used to plan around dynamic obstacles due to their reactive behaviour [20, 21, 22]. The difference between the standard potential field implementations and the one developed for this project was that the repulsive obstacle field at a position  $(x, y)$  was proportional to the cost distribution at  $(x, y)$  for a given time interval. This is shown more formally in Eq. 5.1.

$$U_{rep}(p, t_0, t_m, A) = k \cdot P(p_x, p_y, t_0, t_m, A) \quad (5.1)$$

In Eq. 5.1, the function  $P$  is defined in Eq. 6.2, and  $k > 0$  is a constant. The attractive potential field was kept the same as the standard potential field implementation for robotic motion planning as shown in Eq. 5.2

$$U_{att}(p, g) = c \cdot \|p - g\|^2 \quad (5.2)$$

In Eq. 5.2,  $c$  is a scaling constant such that  $c > 0$ . The potential field planner would use the sum of these two fields to measure the potential through the environment in order to eventually reach the goal by successively moving to the area within the robot's sensing radius that had the minimal potential. Algo. 1 describes more formally how the potential field planner generates a path through the environment.

Through some qualitative testing, these types of potential fields were still leading the robot into unsafe areas and caused the robot to collide with the dynamic obstacles regardless of velocity of the obstacles and the velocity of the robot. After some manipulation of the constants used for the repulsive and attractive potentials, there was only a nominal improvement which lead the author to move towards sampling based motion planning techniques which are outlined in Sec. 5.3 and Sec. 5.4.

---

**Algorithm 1** PF( $q, g, O, A, R$ )

---

```

1:  $q_{min} \leftarrow q$ 
2:  $p_{min} \leftarrow \infty$ 
3:  $\theta \leftarrow 0$ 
4: while  $\theta \leq 2\pi$  do
5:    $q' \leftarrow q + \delta t \cdot s \cdot \text{ROT}(\theta)$ 
6:    $p \leftarrow U_{rep}(q', O \cup A) + U_{att}(q', g)$ 
7:   if  $p < p_{min}$  then
8:      $p_{min} \leftarrow p$ 
9:      $q_{min} \leftarrow q'$ 
10:     $\theta \leftarrow \theta + \delta\theta$ 
11:   for all  $a \in A$  do
12:     STEP( $a$ )
13:   if  $\|q_{min} - g\| < R$  then
14:     return  $\{p_{min}\}$ 
15: return  $\{q_{min}\} \cup \text{PF}(q_{min}, g, O, A, R)$ 

```

---

### 5.3 Space-time Roadmap

The second attempt at devising a solution to the primary objective in Ch. 4 was to create a three dimensional probabilistic roadmap that can capture the connectivity of a two dimensional surface in space-time. A spatio-temporal probabilistic roadmap (PRM) is a directed, weighted graph,  $(V, E)$ , that represents the spatio-temporal connectivity of the search space by randomly sampling points and connecting them such that if  $((i, t), (j, t')) \in E$ , then both  $i$  and  $j$  must not collide with an obstacle at times  $t$  and  $t'$  respectively,  $\|i - j\| \leq d$  where  $d$  indicates the maximum distance between connected nodes can be from one another, there must not be a collision with any obstacle along the edge from  $i$  and  $j$  in the time interval  $[t, t']$ ,  $|t - t'| < \delta t$ , and  $t < t'$  [23, 24]. For the attempted space-time PRM, each node would be a vector,  $(x, y, t)$ , which represents a two dimensional location,  $(x, y)$ , at a certain absolute time  $t$ , and instead of randomly sampling a point in the environment, a node in the graph would be randomly selected and propagated forward in time by some random change in time such that the constraints for the roadmap are still satisfied. This algorithm is shown more formally in Algo. 2.

---

**Algorithm 2** TEMPORALROADMAP( $N, d, \delta t, s, p, O, A$ )

---

**Input:** $n$ : Maximum number of samples $d$ : Maximum distance between neighbouring nodes $O$ : Set of obstacles**Output:**

An weighted directed graph of points describing where it is possible for the robot to move from its initial configuration.

```

1:  $V \leftarrow \{(p, 0)\}$ 
2: for  $i = 1$  to  $N$  do
3:    $(n, t) \leftarrow \text{RANDOMSELECTION}(V)$ 
4:    $t' \leftarrow t + \text{UNIFORMRANDOM}(\varepsilon, \delta t)$ 
5:    $\theta \leftarrow \text{UNIFORMRANDOM}(0, 2\pi)$ 
6:    $q \leftarrow n + s \cdot t' \cdot \text{ROT}(\theta)$ 
7:   if  $\bigwedge_{o \in O} \neg \text{COLLISION}(o, q)$  then
8:     for all  $(v, \tau) \in V$  do
9:       if  $\|v - q\| < d \wedge |\tau - t'| < \delta t$  then
10:         if  $\tau < t'$  then
11:            $E \leftarrow E \cup \{((v, t), (v, t'), C(v, q, \tau, t', A))\}$ 
12:         else
13:            $E \leftarrow E \cup \{((q, t'), (v, t), C(q, v, t', \tau, A))\}$ 
14:      $V \leftarrow V \cup \{(q, t)\}$ 
15: return  $(V, E, W)$ 

```

---

With the generated roadmap, the first thought was to use a graph search algorithm such as A\* [25] or Dijkstra's algorithm [26] to find the path through the environment that had the lowest overall weight. The weight for an edge,  $(i, j)$ , defined as the line integral over the cost surface for a given set of dynamic obstacles with a time interval of  $[i_t, j_t]$ . The notion of a cost distribution is described in Ch. 6 and the formal equation for this line integral is given in Eq. 6.5. This space-time roadmap approach yielded mixed results. The robot would sometimes evade the obstacles, but with the incidence, the planner would lead the robot directly into a collision with a dynamic obstacle. After some testing, it was discovered that since graph search algorithms seek to find the path with minimum combined weight through the graph, these algorithms are biased to return paths with a smaller number of vertices. This is because paths with a larger number of vertices will have a higher overall weight. Since shortest path algorithms try to minimize this overall weight, paths which may be safer but may take longer may not be returned by these algorithms.

To overcome this, instead of searching over the entire graph, the search could occur over the minimum spanning tree of the graph. Since the roadmap is a directed graph, Edmonds' algorithm [27] was used since other minimum spanning tree algorithms such as Kruskal's algorithm [28] and Prim's greedy algorithm [29] only work on undirected graphs. Using the minimum spanning tree would minimize the maximum cost associated with a path from the initial configuration to the goal configuration thus moving the robot away from high cost areas in space-time. Through qualitative analysis, this approach was shown to still lead the robot to high cost areas and even into collisions with obstacles.

This approach using a three dimensional probabilistic roadmap did not work in practice regardless of the search algorithm because of the number of nodes that need to be sampled in space-time in order for it to be effective. The roadmap indicates where in the environment the robot is able to travel to from a starting location in space-time. If the number of nodes is too small the, the goal may not even be in the graph, and thus the robot will never reach it. Also, the less nodes in the graph the less optimal the generated path is, but the more nodes added to the graph, the more computationally difficult it becomes to search. Lastly, the main flaw with this approach is that it biases the sampling to areas that already have a high density of and therefore may not sample nodes in the goal region until sufficiently many samples have been made.

## 5.4 Probabilistic Roadmap With Best First Search

After consideration for other sampling based motion planning techniques such as rapidly exploring random trees [19] and expansive space trees [30] the author chose to explore using a custom graph search algorithm over a two dimensional probabilistic roadmap due to the lack of ability for classical sampling based techniques to deal with time-dependent edge costs. The idea was to use a probabilistic roadmap to capture the connectivity of the two dimensional environment and to generate a search tree through the roadmap that encodes the temporal information for each point in a tree node and is therefore able to account for time-dependent edge costs. This graph search algorithm is a temporal analogue of best-first search which tries to expand the best current node in a search tree based on some heuristic [31]. The heuristic in this project is to expand the node in the search tree that has the minimum cost as defined in Eq. 6.5. A more complete and in depth description of this method is given in Ch. 6.

# CHAPTER 6

---

## Planner Methodology

---

As described briefly in Sec. 5.4, the final planner design uses a probabilistic roadmap to capture the connectivity of the environment and uses a novel variant of best first search to find a safe, low cost path to the goal. This approach is called Dodger. This section describes the algorithm as well as formalizes the definition of a dynamic obstacle and its associated cost distribution and motion.

## 6.1 Dynamic Obstacles

As a major component of this work, dynamic obstacles need to be designed such that one can describe their trajectories, initial configurations, and their levels of uncertainty. This section introduces the definition of a dynamic obstacle used throughout this work along with how one is represented to the planner and its simulated & predicted equations of motion. Specifically, the formal definition of a dynamic obstacle will be introduced, a novel way of representing obstacles using a cost distribution will be formalized, and their predicted and simulated motion will be described.

### 6.1.1 Definition

A dynamic obstacle is defined as a 5-tuple,  $a = (I, \dot{\zeta}, \epsilon, \xi, T)$  where  $I$  is the initial configuration of the obstacle,  $\dot{\zeta}$  is a function,  $\dot{\zeta} : \mathbb{R}^+ \rightarrow \mathbb{R}^2$ , representing the velocity of the obstacle,  $\epsilon$  is used to define a random variable  $\rho \sim \mathcal{U}(-\epsilon, \epsilon)$  that is used to inject noise into an obstacle's trajectory shown in Eq. 6.4 where  $\mathcal{U}$  is a uniform distribution,  $\xi$  is the current configuration used for prediction, and  $T$  is the time that the obstacle was in configuration  $\xi$ . The variables  $\xi$  and  $T$  are dynamic variables and are updated throughout the execution of the algorithm and are used to determine when it is appropriate for the algorithm replans and finds a new path through the environment using more up to date information. This is explained in Sec. 6.2. The variables  $\xi$  and  $T$  are initially set to  $I$  and 0 respectively. It is assumed that the robot has access to this information about the dynamic obstacles and will use it to safely move around them. Information such as the initial configuration and the velocity equation for each dynamic obstacle are assumed to be determined by an external system that is either using a machine learning technique to deduce these properties by using information about where the dynamic obstacle has been before or by an external planning system such as in a warehouse that is commanding the velocities and configurations of these dynamic obstacles. This is the same assumption as that made by Phillips et al [12] and Narayanan et al [11].

### 6.1.2 Cost Distribution

Unlike in the previous work, dynamic obstacles are represented by cost distributions that resemble probability density functions. The difference being is that these cost distributions do not have a unit integral. These cost distributions are used to describe where the obstacle is going to be in within a time interval and can be generated by a third party system, such as a motion capture system. There is an assumption that for a given interval,  $\mathcal{T} = [t_0, t_m]$ , the highest cost with the smallest uncertainty will be at  $t = t_0$  and the lowest cost with the highest uncertainty will be at  $t = t_m$ . Under this assumption, the cost function models how the obstacle may diverge from its current trajectory as time increases. With these assumptions, the cost function,  $P_a : \mathbb{R}^2 \times (\mathbb{R}^+)^2 \rightarrow \mathbb{R}$ , represents the cost surface for a given dynamic obstacle,  $a$ , within a given time interval. Eq. 6.1 formally defines the cost function for a single obstacle.

$$P_a(x, y, t_0, t_m) = \frac{1}{t_m} \cdot \int_{t_0}^{t_m} \mathcal{N}(\zeta_a(t), \alpha \cdot (t - t_0)^2 + \beta, x, y) \cdot (t_m - t)^\gamma dt \quad (6.1)$$

In Eq. 6.1,  $\mathcal{N}(\mu, \sigma^2, x, y)$  is the evaluation of a 3D normal distribution centered at  $(\mu_x, \mu_y)$  with a variance of  $\sigma^2$  at  $(x, y)$  and  $\alpha$ ,  $\beta$ , and  $\gamma$  are scaling constants such that  $\alpha > 0$ ,  $\beta > 0$ , and  $\gamma \geq 1$ . Fig. 6.1 shows an example of  $\mathcal{N}$ . The normal distribution works as a basis function to describe the possible trajectories of the dynamic obstacle. This equation models how the uncertainty of obstacle trajectory prediction increases over time by increasing the standard deviation of the Gaussian distribution as the time increases. Likewise, this function multiplies the Gaussian distribution by a factor of  $(t_m - t)^\gamma$  where  $\gamma \geq 1$  which gives higher costs to times closer to  $t_0$ .

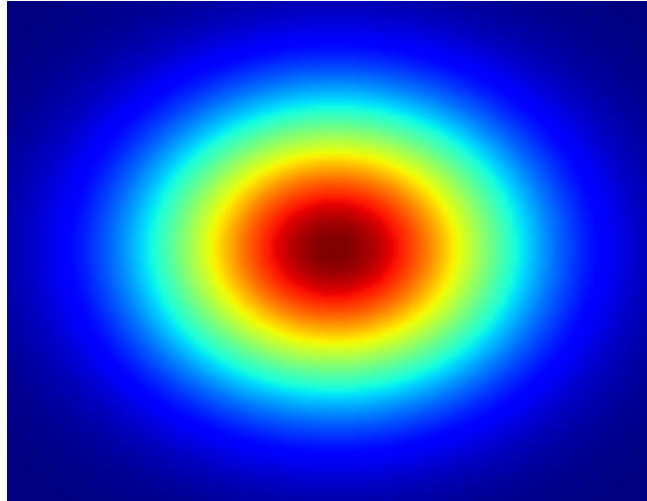


Figure 6.1: A plot depicting the three dimensional normal distribution  $\mathcal{N}(\cdot)$  that is used as a basis function for the obstacle cost distribution. The more red an area, the higher the cost. The more blue an area, the lower the cost.

A cost function is also needed that can incorporate the cost distributions for multiple dynamic obstacles within the environment. The cost function used in this work,  $P : \mathbb{R}^2 \times (\mathbb{R}^+)^2 \times \mathcal{A} \rightarrow \mathbb{R}$  where  $\mathcal{A}$  is the set of all possible sets of dynamic obstacles, calculates the average cost at a point  $(x, y)$  within a given time interval for a given set of dynamic obstacles,  $A$ . This is shown formally in Eq. 6.2.

$$P(x, y, t_0, t_m, A) = \frac{\sum_{a \in A} P_a(x, y, t_0, t_m)}{|A|} \quad (6.2)$$

An example of how  $P$  changes over time is shown in Fig. 6.2. In that example, two dynamic obstacles are placed in the scene and given sinusoidal velocities. In this example the time interval,  $\delta t$ , is kept

constant throughout the simulation, i.e.  $t_m = t_0 + \delta t$ , for all  $t_0 \in [0, T - \delta t]$  where  $T$  is the length of the simulation. Since the velocity does not remain constant in the example, the cost distribution elongates and shrinks based on the acceleration of the obstacle. For instance, in the first and last images in Fig. 6.2, the cost is contained to a small area due to the velocity equations of the obstacles being at their minimum and in the fourth image, the cost is more spread out through the environment because the velocity is at its maximum.

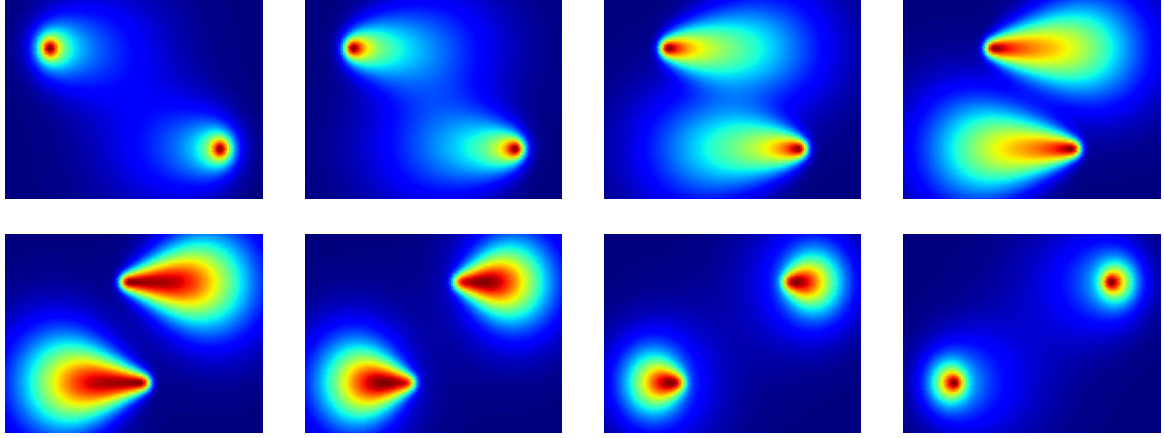


Figure 6.2: Cost distributions indicating the likelihood that a dynamic obstacle will be at a certain location within a given time interval. These figures show how this distribution changes over time. The sequence progress from left to right, top to bottom

### 6.1.3 Equations of Motion

The motion of a dynamic obstacle is defined by the velocity equation, the initial configuration, and the amount of uncertainty. Defining the obstacle's trajectory in terms of its velocity makes it easier to model when creating scenes. The equation of motion for the dynamic obstacle is shown in Eq. 6.3.

$$\zeta_a(t) = \begin{cases} \xi_a + \int_{T_a}^t \dot{\zeta}_a(\lambda) d\lambda & \text{if } t \geq T_a \\ \tilde{\zeta}_a(t) & \text{if } t < T_a \end{cases} \quad (6.3)$$

In Eq. 6.3,  $\tilde{\zeta}_a$  represents the observed trajectory of the obstacle whereas  $\zeta_a$  corresponds to the predicted trajectory of the obstacle. This disambiguation is needed because the planner needs to be able to extrapolate the future movements of a dynamic obstacle. The variables,  $\xi_a$  and  $T_a$  are initially set to  $I_a$  and 0 respectively and are dynamically updated when the algorithm replans. The need for this and how it is designed will be discussed in Sec. 6.2

For the experiments, the motion of the obstacles is simulated by adding a random variable,  $\rho \sim \mathcal{U}(-\epsilon, \epsilon)$  to the trajectory during the numerical integration of the velocity equation. This form of stochasticity allows the obstacle to diverge from its specified trajectory whilst maintaining the same velocity equation. This means that the obstacle will not exhibit random, Brownian motion around its specified path, but rather is able to diverge completely. Also, by adding the random variable to the velocity equation during the numerical integration, the obstacle will not "jump" to a new location, but will gradually diverge off of its specified path. The definition of  $\tilde{\zeta}_a$  is shown in Eq. 6.4. For this equation, it is assumed that the function only computes a value for any given time value,  $t$ , only once.

$$\tilde{\zeta}_a(t) = \begin{cases} \tilde{\zeta}_a(t - \delta t) + \dot{\zeta}_a(t) \cdot \delta t + \rho & \text{if } t > 0 \\ I_a & \text{if } t = 0 \end{cases} \quad (6.4)$$

In Eq. 6.4,  $\delta t$  is a constant where  $\delta t > 0$  and is used for the numerical integration of the velocity. Numerical integration is used in order to allow the path to diverge. Since a recursive function is used for determining the current position of the obstacle, the obstacle's next location will be determined by its last location, its velocity, and a certain error factor  $\rho$ . This will allow the obstacle to exhibit more than simply Brownian motion along a path and it will be able to diverge completely from its specified path. This type of uncertainty is important because it is exhibited in real-world scenarios such as error propagation in controls and by simply not having enough information about the actual velocity equation for a given obstacle. The full extent of  $\tilde{\zeta}_a$  is not known by the planner and this equation is only used to simulate the motion of the obstacles for experimentation and evaluation of the developed planner.

By increasing the level of stochasticity,  $\epsilon$ , for a given dynamic obstacle, it will be more likely to diverge from its current path. This means that the uncertainty of a given dynamic obstacle can be parametrized by its value for  $\epsilon$ .

The motion of a dynamic obstacle is described by its velocity and a starting location in order for the planner to be able to continue to predict an obstacle's motion even when it diverges from its current path. If the obstacle's motion was described by parametric equations of its position, it would not be possible to continue to predict where it is going to move once it is no longer following its prescribed path since the obstacle may diverge from this path completely.

#### 6.1.4 Available Information

It is important to note what information is available to the planner. It is not assumed that the planner has perfect information about the motion of the obstacles or their associated definitions. The planner only has access to the obstacles' velocity equations and their positions throughout the execution of path. The planner does not know the amount of noise,  $\epsilon$ , being injected into the obstacles' velocities as described in Sec. 6.1.3. It is also assumed that the robot or an external system is evaluating the cost distribution based on the predicted motion of the dynamic obstacles in the future. Even though these assumptions may seem unrealistic, there are currently methods being developed that are able to extrapolate and predict the motion of obstacles based on their past locations or based on the algorithm used to dictate their behaviour [32, 33, 34, 35, 36, 37]. Also, as described in Sec. 6.2.4, the planner does not need to have a perfectly precise equation for the obstacles' motion because the planner has the ability to construct a new plan through the environment if the prediction of the obstacles' motion does not accurately depict where the actual location of the obstacle.

## 6.2 Planning Algorithm

The planning algorithm for Dodger has three major components. First, a two dimensional probabilistic roadmap is constructed over the search space in order to capture the spatial connectivity of the environment. The planner then uses a best-first (BestFS) graph search algorithm to determine the safest path from the initial position to the goal position by creating a temporal search tree through the graph in order to account for time-dependent edge costs. Once the robot has an initial path to follow, it will incrementally pursue this path whilst updating its information about the location of the dynamic obstacles. If any of the obstacles deviate from their predicted path, the planner will generate a new path (replan) for the robot using this information. These three components allow the planner to reduce the number of samples over time by reusing the same two dimensional roadmap and allows the planner to account for dynamic obstacles with stochastic motion by replanning. These are improvements to the first sampling based technique described in Sec. 5.3

### 6.2.1 Building the Roadmap

The first component of the planning algorithm is the underlying two dimensional roadmap which represents the spatial connectivity of the environment. This roadmap is constructed using a standard variant

of the probabilistic roadmap algorithm created by Kavraki et al [23]. A probabilistic roadmap is an undirected graph,  $(V, E)$ , created by randomly sampling  $n$  configurations in the configuration space of the robot and connecting them such that if  $(i, j) \in E$ , then  $\|i - j\| < d$ , both  $i$  and  $j$  are not within any of the static obstacles, and there is no collision along the geometric edge from  $i$  to  $j$ . In this work the configuration space is  $\mathbb{R}^2$  and the edge between two nodes is a straight line. The nodes in the roadmap represent the possible configurations of the robot and in this work, points along the edge between two nodes represent geometric transitions from one node to another. The complexity of the graph is parametrized by the number of samples,  $n$ , and the maximum distance between nodes,  $d$ . By increasing the number of samples, the density of samples increases and therefore the average degree for a node in the graph increases. Likewise, if the maximum distance between nodes increases, so does the average degree for a node in the graph. Pseudocode is provided for constructing a probabilistic roadmap in Algo. 3.

---

**Algorithm 3** ROADMAP( $n, d, w, h, O$ )

**Input:**

$n$ : Maximum number of samples

$d$ : Maximum distance between neighbouring nodes

$O$ : Set of obstacles

**Output:**

An unweighted graph of points describing the connectivity of the environment

```

1: for  $k = 1$  to  $n$  do
2:    $q \leftarrow \text{RANDOMPOINT2D}(w, h)$ 
3:   if  $\bigwedge_{o \in O} \neg \text{COLLISION}(o, q)$  then
4:      $V \leftarrow V \cup \{q\}$ 
5:   for all  $i \in V$  do
6:     for all  $j \in V$  do
7:       if  $i \neq j \wedge \|i - j\| \leq d \wedge \bigwedge_{o \in O} \neg \text{COLLISION}(o, i, j)$  then
8:          $E \leftarrow E \cup \{(i, j)\}$ 
9:   return  $(V, E)$ 
```

---

In Algo. 3, first at most  $n$  points are sampled and added to the set of vertices,  $V$ , if and only if there is not a collision with any of the static obstacles. Essentially the Cartesian square of  $V$  is iterated over and any two points that are not the same, whose distance is less than  $d$ , and if there is no collision along the edge between these two points are added to the edge set,  $E$ . Finally, the vertices and edges are returned as a tuple representing the graph. Fig. 6.3 shows a constructed probabilistic roadmap with 300 nodes.

### 6.2.2 Searching the Graph

To search the generated two dimensional probabilistic roadmap in space-time, a novel best first search (**tBestFS**) algorithm has been developed that creates a search tree that expands the current node not only in space but also in time until the current node is within an acceptance radius of the goal. This algorithm works by using a priority queue to store the expanded nodes. The priority is based on two things, how many times a two dimensional node in the probabilistic roadmap has been expanded and the cost to reach the node in space-time in the queue. A dictionary indexed by the node and mapped to an integer is used to keep track of how many times the node has been visited. The cost between two nodes in space-time,  $(i, t)$  and  $(j, t')$  is defined by the line integral from  $i$  to  $j$  over the exponential of the cost distribution  $P$  for the time interval  $[t_0, t_m]$  and set of dynamic obstacles  $A$ . This function uses the exponential of the cost distribution in order to emphasize higher costs along the path. This is formally shown in Eq. 6.5.

$$\begin{aligned}
 C(i, j, t_0, t_m, A) &= \int_0^1 \exp \left( P(x(\lambda), y(\lambda), t_0, t_m, A) + 1 \right) \cdot \sqrt{\left( \frac{dx}{dt} \right)^2 + \left( \frac{dy}{dt} \right)^2} d\lambda \\
 &= \int_0^1 \exp \left( P(x(\lambda), y(\lambda), t_0, t_m, A) + 1 \right) \cdot \sqrt{(j_x - i_x)^2 + (j_y - i_y)^2} d\lambda \\
 &= \int_0^1 \exp \left( P(x(\lambda), y(\lambda), t_0, t_m, A) + 1 \right) \cdot \|i - j\| d\lambda
 \end{aligned} \tag{6.5}$$

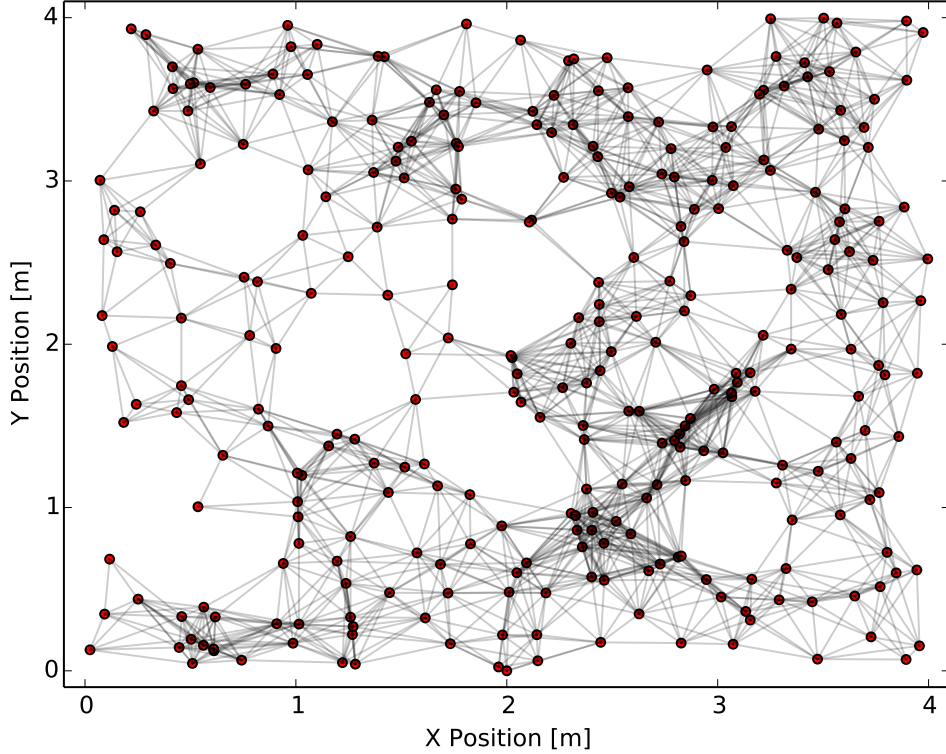


Figure 6.3: An example of a probabilistic roadmap generated in free space without the presence of obstacles. The nodes are represented by the circles and the red line as the edges between the nodes.

In Eq. 6.5,  $C$  is a function  $C : \mathbb{R}^2 \times \mathbb{R}^2 \times (\mathbb{R}^+)^2 \times (\mathbb{R}^+)^2 \times \mathcal{A} \rightarrow \mathbb{R}$  where  $\mathcal{A}$  is the set of all possible sets of dynamic obstacles, and  $x(\lambda) = (j_x - i_x) \cdot \lambda + i_x$  and  $y(\lambda) = (j_y - i_y) \cdot \lambda + i_y$  are the parametric equations of the line from  $i$  to  $j$ . Eq. 6.5 increases exponentially as the maximum cost along the line increases and therefore makes edges with larger maximum costs more costly than edges with lower maximum costs. To combine the two cost formulations for an edge,  $((i, t), (j, t'))$ , a weighted sum is computed that adds the number of times node  $j$  has been visited with the line integral over the cost distribution from  $i$  to  $j$  for the given time interval. This total cost function is formally described in Eq. 6.6.

$$TC(i, j, t_0, t_m, A, D) = \psi \cdot C(i, j, t_0, t_m, A) + \omega \cdot D_j \quad (6.6)$$

In Eq. 6.6,  $\psi$  and  $\omega$  are scaling constants. It is important to incorporate a penalty for returning to a location that has already been visited even if this penalty is small because the tBestFS algorithm may choose to only expand nodes in a safe area and thus not reach the goal since there is not a heuristic to sample nodes closer to the goal in order give preference to safer paths instead of shorter ones.

Since the algorithm operates in both space and time, the search tree is expanded at a given node,  $i$  at a time  $t$ , by determining how long it would take the robot to reach all of the neighbours of  $i$  and not only adding each neighbour of  $i$  into the priority queue with its associated cost, but also adding the time at which the robot would reach each neighbour. This is accomplished by assuming the robot will travel at a constant speed,  $s$ , through the environment which makes it easy to compute how long it would take the robot to reach a neighbour,  $j \in \text{NEIGHBOURS}(i)$ . The time it would take for the robot to reach a neighbour,  $j$  from  $i$  is  $\|i - j\|/s$  which would make the robot reach  $j$  at time  $t + \|i - j\|/s$ . Also, since the algorithm is also operating in time, the robot is able to stay at the same location for a given wait time  $\delta t$  if it is less costly than moving forward to any of its neighbours.

The algorithm progresses forward by expanding the best current node in the priority queue. This is the node that has the smallest combined cost in the queue. Once a node,  $i$  at time  $t$ , is expanded and its temporal neighbours determined, the parent for each of these neighbours is defined as  $i$  at time  $t$ . By storing the parents of each of the neighbours, it becomes possible to backtrack from the goal to the

starting position once the goal is reached and construct a path to the goal configuration. The algorithm terminates either when there are no more nodes in the priority queue or once the node popped out of the queue is less than a certain distance away from the goal node. Once the node popped out of the priority queue is within the goal region, the path to the goal is returned. The algorithm used for searching the graph is described formally in Algo. 4.

---

**Algorithm 4** tBestFS( $V, E, R, A, p, g, T$ )

---

```

1:  $Q \leftarrow \text{PRIORITYQUEUE}()$ 
2:  $D \leftarrow \text{DICTIONARY}()$ 
3:  $\mathcal{P} \leftarrow \text{DICTIONARY}()$ 
4:  $\text{INSERT}(Q, p, T)$ 
5: while  $|Q| > 0$  do
6:    $(q, t) \leftarrow \text{POP}(Q)$ 
7:   if  $\|q - g\| \leq R$  then
8:     return BACKTRACKPATH( $p, q, t, \mathcal{P}$ )
9:    $S \leftarrow \emptyset$ 
10:   $N \leftarrow \text{NEIGHBOURS}(V, E, q) \cup \{q\}$ 
11:  for all  $n \in N$  do
12:    if  $q \neq n$  then
13:       $t' \leftarrow \|q - n\|/s + t$ 
14:    else
15:       $t' \leftarrow t + \delta t$ 
16:     $\mathcal{P}_{(n,t')} \leftarrow (q, t)$ 
17:     $c \leftarrow \psi \cdot C(q, n, t, t', A) + \omega \cdot D_n$ 
18:     $D_n \leftarrow D_n + 1$ 
19:     $Q \leftarrow \text{INSERT}(Q, (n, t'), c)$ 

```

---

From the algorithm in Algo. 4, it is evident that picking a good wait time,  $\delta t$ , is important for generating safe paths through the environment. Having a large value for  $\delta t$  can lead to very suboptimal paths because even though staying in the same position for a given period of time may be safer than moving to any of the neighbours, staying there for too long could lead the planner to miss safer viable paths. For instance, say the planner has expanded a node,  $i$  at time  $t$  and  $TC(i, i, t, t + \delta t, A, D) < TC(i, j, t, t + \|i - j\|/s, A, D)$  for all  $j \in \text{NEIGHBOURS}(i)$ . There may be a neighbour  $j$  and some time  $t'$  such that  $t < t' < t + \delta t$  where  $TC(i, j, t, t', A, D) < TC(i, i, t, t + \delta t, A, D)$ . Moving the robot to node  $j$  at time  $t'$  from  $i$  at time  $t$  would lead to a safer path than staying at node  $i$  until time  $t + \delta t$ . This is why it is important for the safety of the generated paths to use a small value for  $\delta t$  in order to not miss sampling safe paths. By using a smaller value for  $\delta t$ , the chance that a safer path would be missed decreases, but the number of nodes in the search tree would increase.

Fig. 6.4 shows how the search tree for tBestFS is being built in space-time as the algorithm progresses. The sequence for this figure is left to right, up to down. The last plot in the Fig. 6.4 also shows the path in red that was returned by tBestFS. Fig. 6.5 shows how the dynamic obstacle cost distribution changes over time for the search tree in Fig. 6.4. In Fig. 6.4, the tree is being expanded into areas that have low cost in space-time and that is why the tree is being expanded on the left of the scene. It is evident that the tree is essentially moving around the dynamic obstacles when they are all near each other on the right side of the scene.

### Completeness

It is important to prove certain properties about the completeness of the tBestFS algorithm in order to guarantee that the algorithm will always return a path in a finite amount of time. For the completeness proof it is first important to prove properties about the bounds of the two functions that comprise the total cost function for an edge. The proof for completeness rests on the fact that the added penalty of returning to a node will be monotonically increasing as the number of times the node has been visited increases and that the cost of an edge is strictly finite for all acceptable parameters. The proof uses these properties to show that in a finite amount of time, it will be more favourable to expand towards the goal node than to stay in the same location.

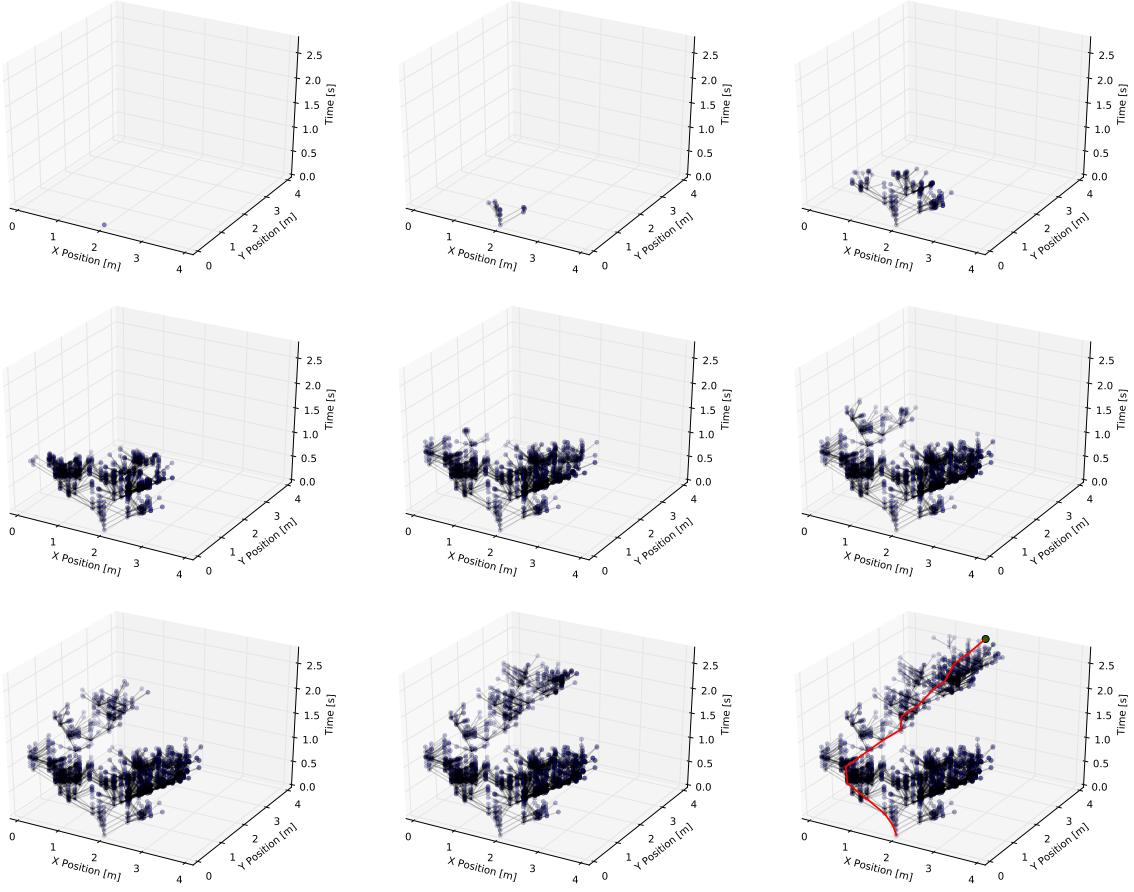


Figure 6.4: A depiction of the search tree generation for a given probabilistic roadmap. The  $x$  and  $y$  axes represent the  $x$  and  $y$  location of the node, and the vertical axis represents time. The sequence progress from left to right, up to down. The final image in sequence also shows the path taken by the robot in red.

**Lemma 1.** *The added penalty of returning to a node in the probabilistic roadmap is monotonically increasing.*

*Proof.* Since the added penalty for returning to a node increases by one each time the node is visited, as the number of times it has been revisited increases to infinity, so does the added penalty. □

**Corollary 1.** *The total cost,  $TC$ , is a monotonically increasing function.*

The second property of the functions that make up the edge cost is shown in Lemma 2 which describes that the cost function,  $C$  will always have a value less than infinity for all permissible parameters.

**Lemma 2.** *The cost for any  $(m, n) \in E$  for a time interval  $[t, t']$  such that  $t' - t < \infty$  is strictly less than infinity and  $0 < t < t'$ .*

*Proof.* The function,  $C$ , can only increase to infinity if the two nodes on the edge are an infinite distance apart or if the cost distribution in Eq. 6.1,  $P$ , increases towards infinity. For the former, two nodes cannot be an infinite distance apart because the connection distance,  $d$ , is set to be strictly less than infinity and because the  $\forall i, j \in V : ||i - j|| \leq \sqrt{w^2 + h^2}$  where  $0 < w < \infty$  and  $0 < h < \infty$  are the width and height of the scene respectively. Therefore  $C$  cannot tend to infinity because of the distance between nodes since no two nodes are an infinite distance away. For the latter,  $P$  can only tend to infinity if the normal distribution,  $\mathcal{N}$  reaches infinity. This is only possible if the variance approaches 0. However the

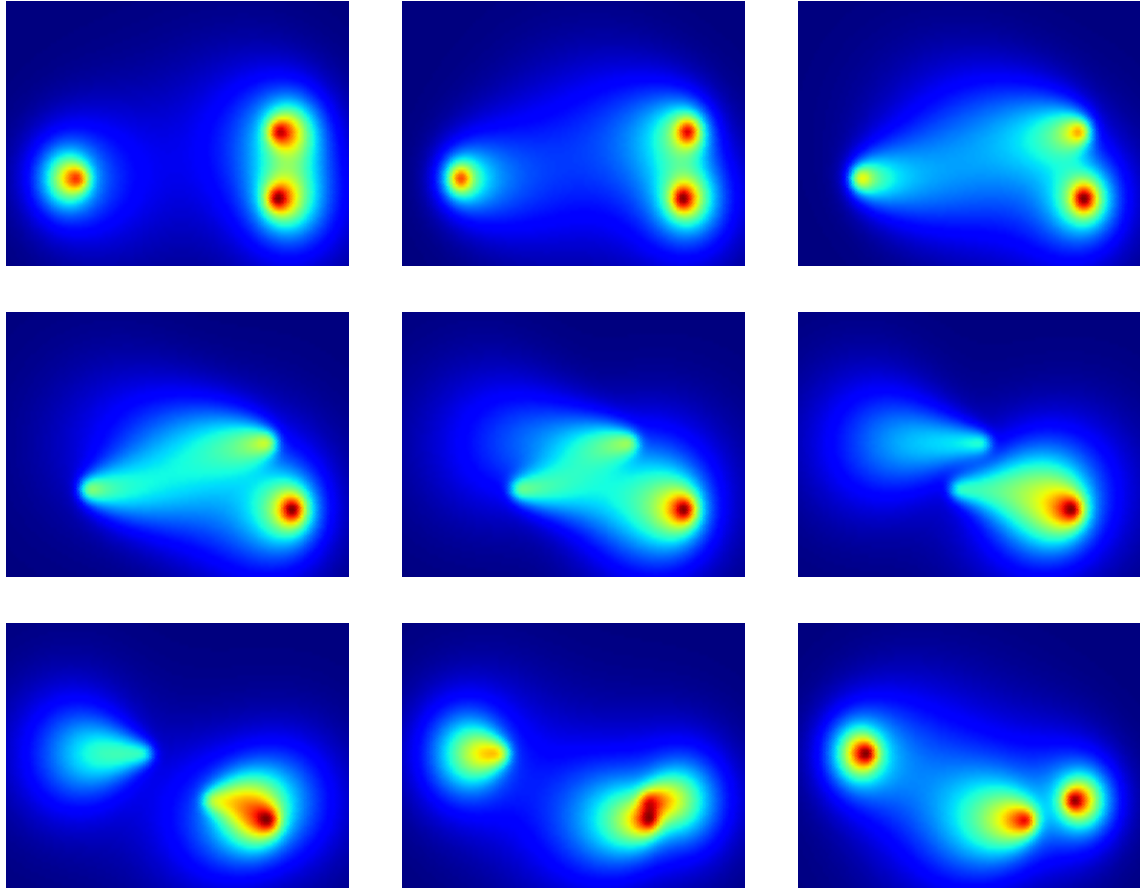


Figure 6.5: A sequence of images showing the progression of the cost distribution for the set of dynamic obstacles over time used for the search tree shown in Fig. 6.4. The sequence progresses from left to right, up to down.

variance cannot reach 0 in this case because the constant  $\beta$  is always greater than zero. Therefore it is impossible for the cost along an edge,  $C$ , to tend towards infinity.

□

Using Lemmas 1 and 2, a proof can be constructed for Theorem 1 which states that `tBestFS` is complete and will always return a path.

**Theorem 1.** *`tBestFS` will always return a path in a finite amount of time.*

*Proof.* First, it is important for the proof to note that the penalty for returning to a previously visited location increases monotonically to infinity as the number of visits for a particular node approaches infinity. Also, the cost function,  $C$ , is bounded strictly below infinity for all possible parameters. Now assume the pathological case where  $\forall(m, n) \in E, \forall i \in \text{NEIGHBOURS}(g) : C(i, g, t, t', A) > C(m, n, t, t', A)$  for all time intervals  $[t, t']$  and where  $g$  is the goal node in the probabilistic roadmap. This means that the cost to reach the goal will be larger than any edge cost at any time in the graph. Therefore, without the added penalty for returning to a previously visited location, the goal will never be popped out of the priority queue for expansion. However, since there is a penalty for returning to the same geometrical location, as the algorithm progresses,  $\forall(m, n) \in E, \forall i \in \text{NEIGHBOURS}(g) : TC(i, g, t, t', A, D) < TC(m, n, t, t', A, D)$  because each node in the probabilistic roadmap except the goal node would have been expanded one or more times, thus increasing the added penalty. Since the goal node has not been expanded, its total cost would only be the value for  $C$  and since  $C$  is bounded below infinity and the added penalty increases monotonically towards infinity, all edges to the goal node would have a lower cost than any edge to any

other node and thus the goal would be expanded. If the goal is expanded, a path to the goal would be returned. The path is returned in a finite amount of time because the number of nodes in the graph is finite.

□

### 6.2.3 Replanning

In order to generate safe paths in uncertain, stochastic environments, the planner is not able to simply provide an *a priori* plan from the **tBestFS** algorithm. It is necessary for the planner to generate new paths from the current configuration of the robot as it progresses through the environment if the actual trajectory of a dynamic obstacle deviates too much from its predicted trajectory. This planning occurs in real-time during the execution of the path in the environment. This framework for regenerating paths is called *replanning*. Replanning for this work occurs once the model of movement for a given dynamic obstacle can no longer predict within an acceptable error the actual position of the dynamic obstacle. When replanning, the same probabilistic roadmap is used and the connectivity of the environment is not resampled.

Replanning works by first generating a preliminary path through the environment using the **tBestFS** algorithm. The robot will then follow this path by moving at its prescribed constant speed,  $s$ , in a straight line from node to node in the path. Once it reaches a node,  $i$  at time  $t$  in the path, the robot checks whether the actual locations of the obstacles either sensed by the robot or by an external system differ more than an acceptable amount,  $\delta$ , from the predicted locations of the dynamic obstacles at time  $t$  i.e.

$$\bigvee_{a \in A} \|\tilde{\zeta}_a(t) - \zeta_a(t)\| > \delta$$

Where  $A$  is the set of dynamic obstacles. If this proposition is true, there is substantial deviation in the obstacle positions, the planner will update the value of the dynamic variables,  $T$  and  $\xi$  for the obstacles which are used for predicting their trajectories to  $t$  and  $\tilde{\zeta}_a(t)$  respectively. These variables are part of the 5-tuple defining the dynamic obstacles which is described in Sec. 6.1.1. Once these variables are updated, the graph is searched using the **tBestFS** algorithm starting from the current position of the robot,  $i$  with a starting time of  $t$ . It is also important to note that the same dictionary used for storing how many times a node has been visited when researching the graph. The actual path of the robot is a union of the past locations of the robot based on the partial paths generated whilst traversing the environment. Algo. 5 describes the processes of replanning due to the deviations in the obstacle locations and is the main entry point for the Dodger algorithm.

Replanning is necessary because it allows the planner to redirect the robot to new, safer paths as the environment changes. This is important because the initial path generated by the **tBestFS** algorithm uses the predicted motion of the obstacles and assumes they will stay on this predicted trajectory for the execution of the path. The **tBestFS** is able to account for some uncertainty in the motion of the obstacles as described by the cost distribution in Sec. 6.1.2 but this distribution is not able to fully account for path divergences. By updating the information for the dynamic obstacles and re-searching the probabilistic roadmap using **tBestFS**, safer overall paths can be generated. It is possible to regulate the number of times the planner will need to replan and thus the safety of the plan by adjusting the value for  $\delta$ . The larger the value for  $\delta$ , the more the obstacles will need to diverge from the prescribed trajectories in order for the planner to initiate the replanning sequence and vice-versa.

### 6.2.4 Discussion

The final algorithm developed is able to generate low cost paths through the environment by using the available information about the obstacles' motion. The planner is able to do this by searching through space-time over a two dimensional graph using the **tBestFS** algorithm which uses the cost distribution

---

**Algorithm 5** DODGER( $n, d, w, h, \delta, p, g, O, A, R$ )

---

**Input:**

$n$ : Maximum number of samples for the roadmap  
 $d$ : Maximum distance between neighbouring nodes in the roadmap  
 $w$ : Width of the scene  
 $h$ : Height of the scene

**Output:**

```
1:  $(V, E) \leftarrow \text{ROADMAP}(n, d, w, h, O)$ 
2:  $\Pi \leftarrow \emptyset$ 
3:  $q \leftarrow p$ 
4:  $t \leftarrow 0$ 
5: while  $\|\text{BACK}(\Pi) - g\|_2 > R$  do
6:    $\pi \leftarrow \text{SEARCHGRAPH}(V, E, R, A, q, g, t)$ 
7:   for all  $(i, t') \in \pi$  do
8:      $\Pi \leftarrow \Pi \cup \{i\}$ 
9:     for all  $a \in A$  do
10:     $\text{STEP}(a)$ 
11:    if  $\bigvee_{a \in A} \|\tilde{\zeta}_a(t') - \zeta_a(t')\| > \delta$  then
12:      for all  $a \in A$  do
13:         $T_a \leftarrow t'$ 
14:         $\xi_a \leftarrow \tilde{\zeta}_a(t')$ 
15:         $q \leftarrow i$ 
16:         $t \leftarrow t'$ 
17:      break
18: return  $\Pi$ 
```

---

described in Sec. 6.1.2 to weight the edges of the search tree. The algorithm is also able to adapt and create new plans through the environment when its' prediction of the obstacles' motion is no longer able to accurately determine where the obstacles are going to be in future. This replanning stage of the algorithm allows it to be used in real-time in stochastic dynamic environments. This mimics the reactive behaviour of potential fields, with the added benefit of provable completeness and not being a solely reactive planner. Likewise, the replanning ability allows the information given to the planner about the motion of the obstacles not to be perfect. Even if the equations of motion that the motion prediction system provides in no way describe the actual motion of the obstacles, the algorithm will simply replan at every time step and instead of using the cost distributions to determine paths through the environment, the planner will simply move to the next best node in the probabilistic roadmap. This means that the algorithm is able to continuously plan through stochastic dynamic environments utilizing the available information to move the robot to the goal.

# CHAPTER 7

---

## Implementation

---

### 7.1 Initial

Due to the ease of development and the author's experience with the language, Python was chosen as the initial language for the implementation. All three attempts described in Ch. 5, were implemented and a suite of tests scripts and visualization mechanisms were created in order to incrementally assess how each planner was behaving. However after the implementation was completed for the final design described in Sec. 5.4, it was discovered that Python could not produce solution paths (without replanning) through dynamic environments in a real-time scenario. Since Python could not search the graph within an acceptable amount of time, it could only be used for *a priori* planning and therefore could not be used in stochastic environments in which replanning would be needed. Due to this drawback, the author decided to rewrite the entire implementation in C++. Since this initial attempt is complete, it is publicly available at [38].

### 7.2 Final

The final implementation was written in C++ due to the tremendous speed improvement which made planning in real-time viable. Due to the object oriented structure of C++, the planner and the associated data structures were encapsulated in classes which made it very easy for people to use the code as an API. While designing the software, extra effort was put into making the code easily usable by other people who are not necessarily experts in robotics or motion planning. The system has an easy import mechanism and several examples on how to use the different planners that have been implemented.

In order to visualize the paths that the planner has generated, the C++ code can export the paths of the robot and the dynamic obstacles to a JSON file and a Python script then can read and parse the generated JSON and display the paths using either Matplotlib or RViz. Matplotlib is an open source library for creating plots from data [39]. It is very similar to Matlab or Mathematica except it runs natively in Python. RViz is a core component of the Robotic Operating System (ROS) which can render dynamic scenes in three dimensions and can visualize native geometrical and navigation messages from ROS [40]. Since the paths are exported to JSON, a standard format with parsers in many languages, third party software can be developed that can parse the generated JSON file and analyze or visualize the generated paths. Likewise, the Dodger library can be imported by a third party program to control robots from the generated paths or to visualize the paths using other visualization tools such as OpenGL.

A diagram of this tool-chain is shown in Fig. 7.1.

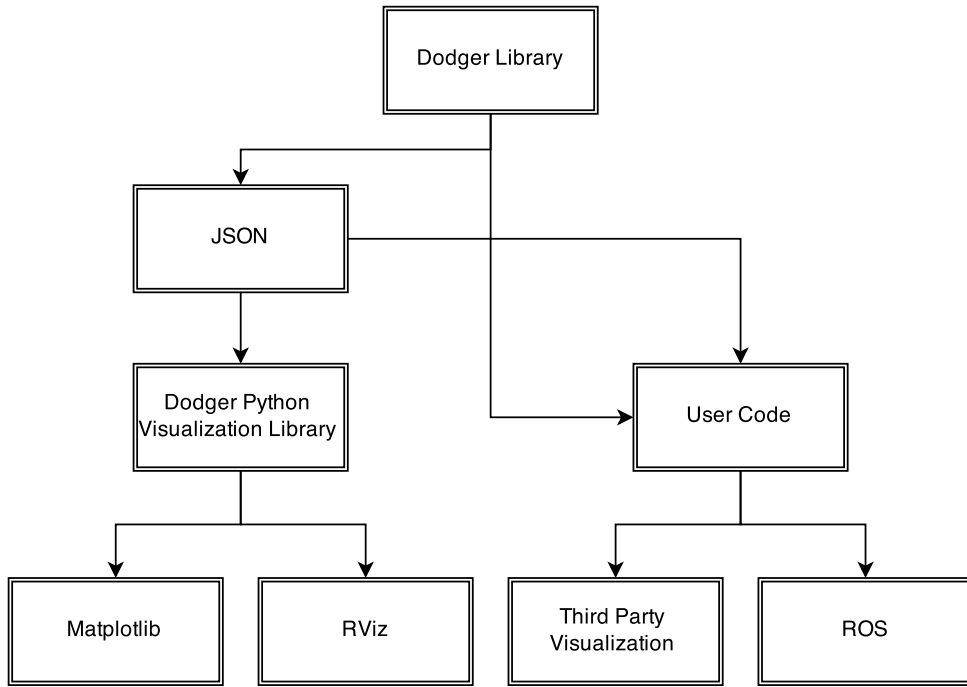


Figure 7.1: A diagram depicting the work flow for the implementation. The Dodger library can either generate a path and export to a JSON file which can then be visualized in Matplotlib or RViz using one of the Python scripts provided or user code can read the exported JSON to control robots or visualize the paths. The library can also be imported by user code to either visualize paths or control a robot with ROS.

By separating the visualization code completely from the planner code, the software is more easily portable to different visualization frameworks and ensures that the user does not need to have a certain graphical software or ROS installed for the software to be able to compile and use the library. This allowed the planner code to be entirely self contained and simple to compile with a provided CMake file which compiles the C++ code into a static library. Likewise, this design decision in the implementation allows the generated paths to be saved and either analysed or visualized at another time. Also, since the planner had no dependencies, experiments could be run on the servers provided without needing root access. This code is also made publicly available at [41].

# CHAPTER 8

---

## Experimental Setup

---

### 8.1 Design

In order to quantify the performance of the developed planner and to judge how well it performs, experiments needed to be run that can determine the degree of safety present in the generated paths and how long it takes to generate these paths. To gather this data, three different scenes were created with differing number dynamic obstacles with different trajectories. The independent variables, or parameters, for each scene consisted of the amount of noise,  $\epsilon$  for the dynamic obstacles and the speed of the robot,  $s$ . For the experiments, a given value of  $\epsilon$  is the same for all of the dynamic obstacles in the scene. The amount of noise ranges from 0.002 to 0.01 with an increment of 0.002 and the speed ranges from 1.0 to 4.5 meters per second with an increment of 0.5 meters per second. Due to the stochasticity of the planner and the dynamic obstacles, each set of parameters for each scene was run 20 times. The values for each metric recorded is averaged and the standard deviation for each set of parameters for each scene is presented.

In order to judge how the developed planner compares to a standard algorithm developed to plan in stochastic dynamic environments, a slight variant to the potential fields planner described in Algo. 1 was implemented. The difference is that the implemented potential fields planner used a different repulsive potential function that is described in Eq. 8.1.

$$U_{\text{rep}}(p, t, A) = \max_{a \in A} \frac{k}{||\tilde{\zeta}_a(t) - g||^2 + \varepsilon} \quad (8.1)$$

In Eq. 8.1,  $k$  is a scaling constant where  $k > 0$ , and  $\varepsilon$  is constant where  $0 < \varepsilon < k$  that ensures that the function does not exhibit a singularity. This variant in the potential fields ensures that the planner has no information about the motion of the obstacles and can thus be used to compare how this information can benefit a planner. Also, since this planner is not sampling based, it can be used to see how a complete sampling based planner can be more or less effective. The results from this experimental setup are described in Ch. 9.

## 8.2 Metrics

To quantify the performance of the planners, four metrics are used, three to measure the safety and one for computational time. Along with these metrics, the standard deviation is collected for each scene and set of parameters in order to gauge the reliability of the planner under different circumstances. These metrics are described in the sections below.

### 8.2.1 Safety

In order to quantify the safety of a given path  $\Pi$ , three metrics were devised. These metrics need to be used together to measure the safety of a path and each represent a component of what it means for a path to be "safe". The first metric is the most straightforward and what is probably the first metric to come to mind, the minimum distance to any dynamic obstacle at any given time. This metric represents for a given path, what was the closest the robot came to coming into contact with a dynamic obstacle. Since collisions are more likely to occur as the robot approaches an obstacle due to the uncertainty in its motion, this metric serves to provide a simple way of quantifying the safety without having to account for the motion of the obstacles. This metric is defined formally in Eq. 8.2.

$$\text{MinDist}(\Pi, A) = \min_{t \in \mathcal{T}} \min_{a \in A} \|\zeta_a(t) - \Pi(t)\| \quad (8.2)$$

In Eq. 8.2,  $\Pi$  is the path of the robot,  $\mathcal{T}$  is the time interval for the path, and  $A$  is the set of dynamic obstacles in the scene. Since this metric does not account for the motion of obstacles, it cannot be used as the sole quantification of safety. For example, if the robot moved near a dynamic obstacle, but was moving in the opposite direction of the obstacle, the path taken by the robot would still be safe, because there would be a smaller chance of the robot actually coming into contact with the obstacle. The robot could have a smaller cost over its path even if it moved near an obstacle than a robot that was farther away from an obstacle but moved directly into its trajectory.

Another metric used to compute the safety of a path is the maximum cost incurred by the robot along the path. This is what the planner described in Sec. 6.2 is trying to minimize. This metric describes how risky a certain path is by determining the likelihood that the robot's path would intersect with the trajectory of a dynamic obstacle. A formal definition of this metric is shown in Eq. 8.3.

$$\text{MaxCost}(\Pi, A) = \max_{t \in \mathcal{T}} P(\Pi(t), A) \quad (8.3)$$

Since the potential field planner implementation that is used to compare with the planner created in this work does not utilize the information given about the cost distribution associated with dynamic obstacles, this metric also indicates how access to this information can contribute to generating safer paths through dynamic environments. Since this metric is used to measure the safety of both the potential fields planner and the developed planner, this metric can be used to quantify how information about the motion of dynamic obstacles can either improve or have no effect on the generated paths.

The last metric used to measure the safety of a generated path is the average cost associated with the robot along the path as determined by the cost distribution. This metric does not provide the same indication of safety as in Eq. 8.3 because the overall safety of a path is not just the average safeness along the path. For instance if the majority of a path taken by a robot has a relatively low cost, but then the robot comes into a collision with an obstacle along the path, this path cannot be labelled as safe. However, this metric combined with the metrics described in Eq. 8.3 and Eq. 8.2 can be used to gauge the level of safety for a given path. This last metric is described formally in Eq. 8.4.

$$\text{AvgCost}(\Pi, A) = \frac{1}{\max \mathcal{T}} \cdot \int_{\mathcal{T}} P(\Pi(t), A) dt \quad (8.4)$$

Since experiments were conducted with a given set of parameters multiple times due to the stochasticity of the dynamic obstacles and the developed planner, each of the metrics were gathered for each individual run. The data gathered for each of these metrics was then averaged and the standard deviation of the dataset was determined. As such, it is the averages and standard deviations of these metrics that are used to quantify the safety of a generated path.

### 8.2.2 Computational Time

In order to determine the feasibility of the paths generated by both planners, the amount of computational time needed for each planner was collected. Collecting this data can indicate how well the developed planner can perform in a real-time scenario. Since the time it takes to compute a path with replanning, the computational time also represents how long it would take for the robot to execute the path because it is replanning in real-time.

### 8.2.3 Variance

For each set of parameters, the experiments were conducted multiple times due to the stochasticity of the dynamic obstacles and the planner. The standard deviation for each metric and each set of parameters were recorded and used to indicate how the noise injected into the trajectories of the dynamic obstacles and the speed of the planner affect the variance in the results. This metric provides an indication of how consistent the planners will be for different sets of parameters and can contribute to judging how well each planner will work in a real world scenario over time.

## 8.3 Scenes

Three different scenes were used for testing the algorithms developed. These scenes contain oscillating dynamic obstacles with different configurations and do not contain any static obstacles. No static obstacles were included in the scenes because the ability to navigate around static obstacles is not the objective of this project and it is assumed that if the planner is able to generate paths through dynamic scenes, that they would be able to do so for static scenes. The images on the following pages depict how the dynamic obstacles progress over time for each scene. The dynamic obstacles are depicted as mobile ground robots, and no noise is added to their trajectories for these examples.

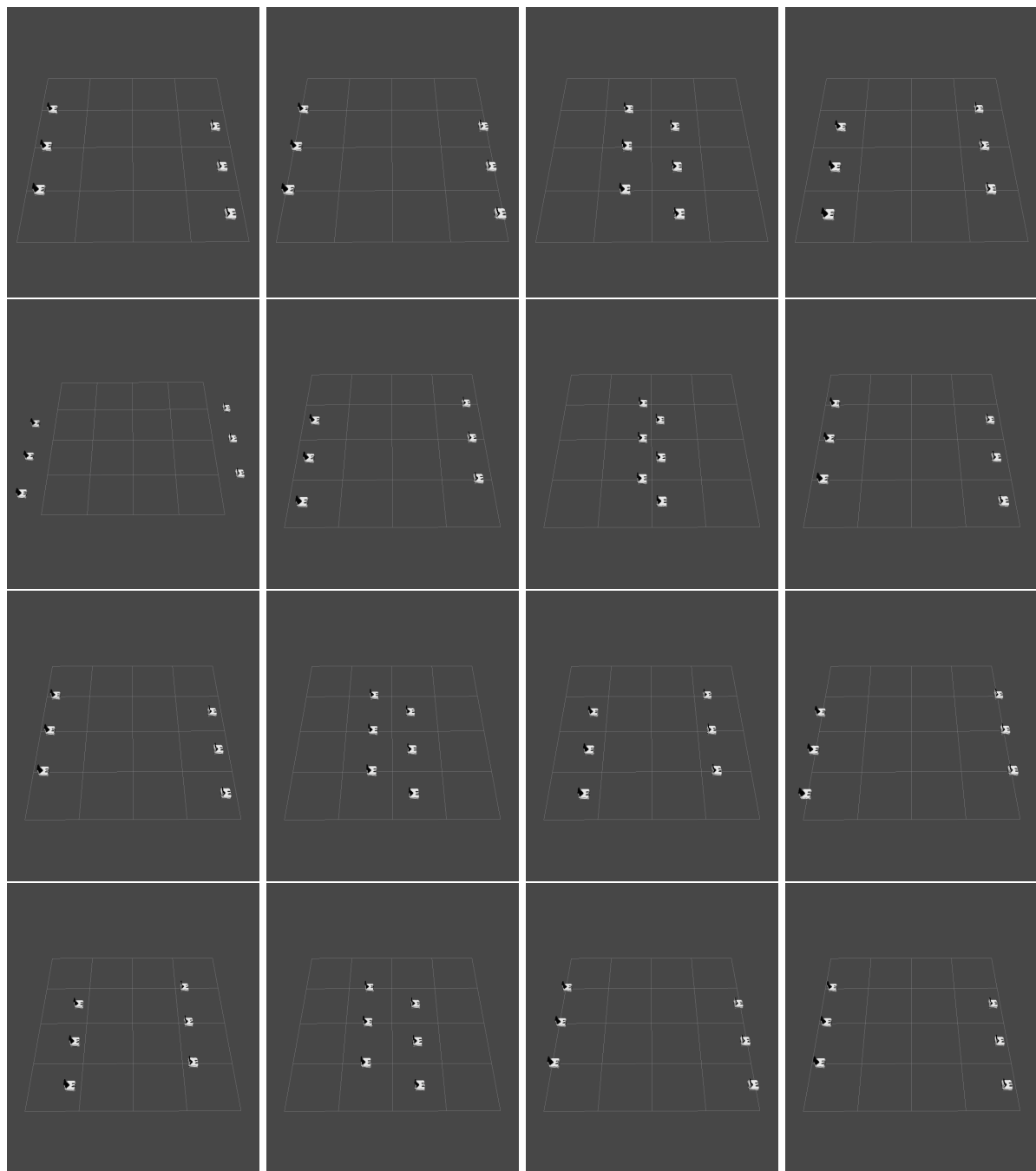


Figure 8.1: A depiction of how the dynamic obstacles progress over time for Scene 1. No noise is added to their trajectories in order to display the pure velocity function used for their motion. The sequences progresses from left to right, top to bottom.

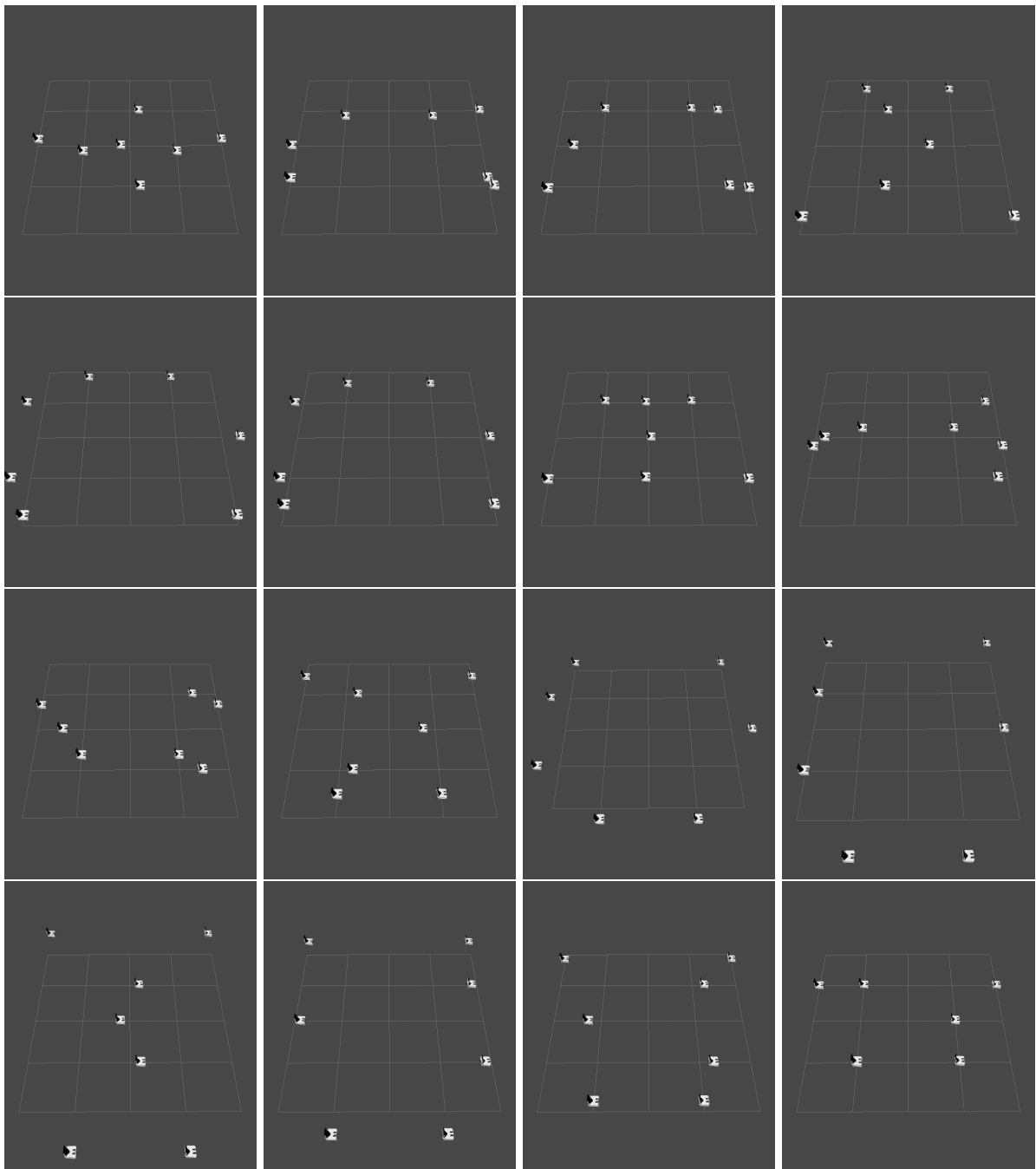


Figure 8.2: A depiction of how the dynamic obstacles progress over time for Scene 2. No noise is added to their trajectories in order to display the pure velocity function used for their motion. The sequences progresses from left to right, top to bottom.

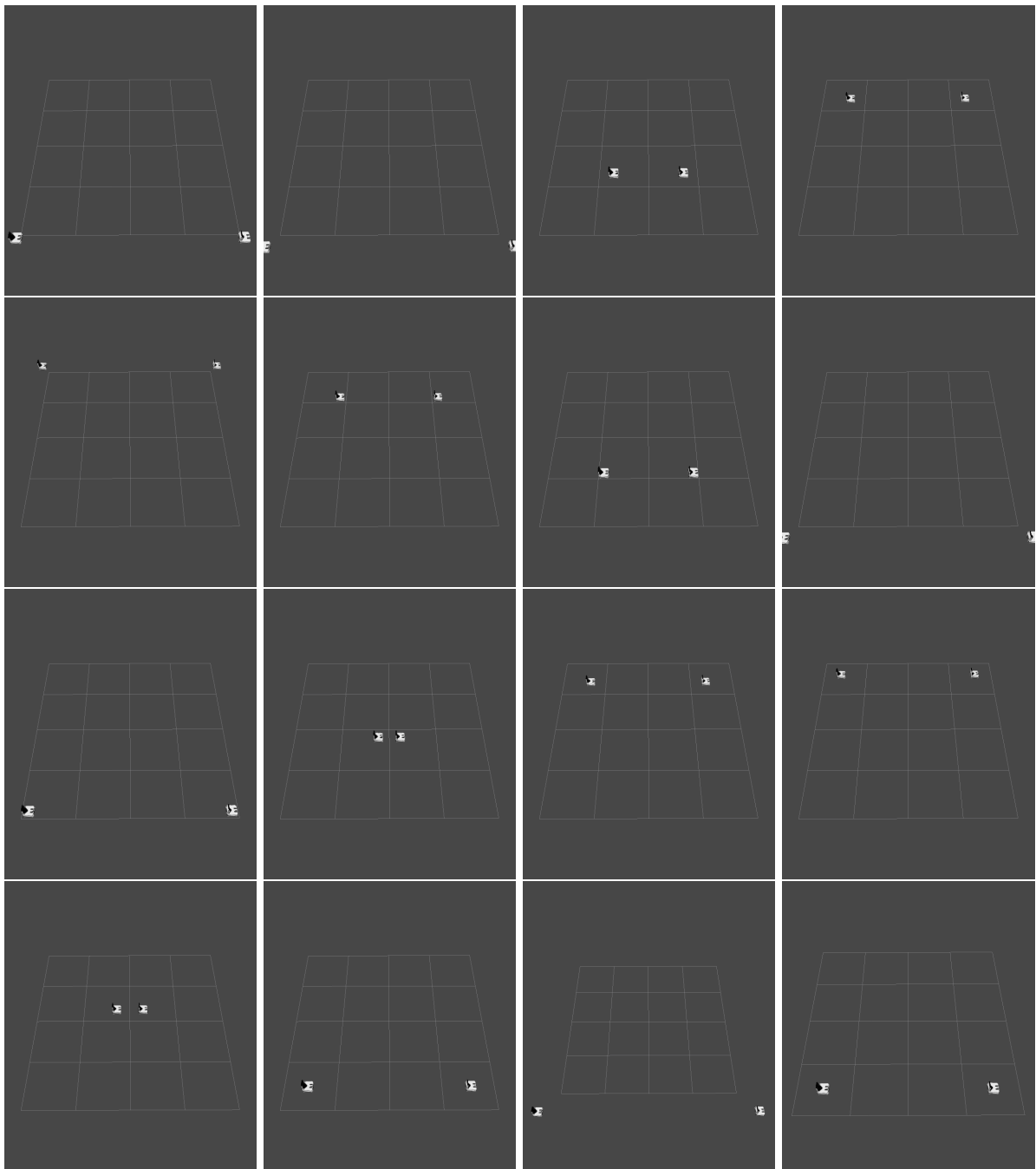


Figure 8.3: A depiction of how the dynamic obstacles progress over time for Scene 3. No noise is added to their trajectories in order to display the pure velocity function used for their motion. The sequences progresses from left to right, top to bottom.

# CHAPTER 9

---

## Results

---

This chapter presents the results from the experimentation of the algorithm. The metrics used and the experimental setup is described in Ch. 8. This chapter will describe the empirical data gathered for the safety and computational time of the algorithm developed in Sec. 6.2. This chapter will also compare the proposed approach with a more standard approach, potential fields, using the empirical data gathered. For all of the plots presented, the data for the algorithm developed in this work is shown on the left and the data for the standard potential fields planner is shown on the right. Also note that this chapter only surveys the results for Scene 1 because the data was very similar for all of the scenes. The plots for the other scenes are shown in the appendix.

### 9.1 Safety

Providing an empirical evaluation of the safety of the developed planner is incredibly important because if it does not provide quantifiable safe paths through the environment, the main objective was not satisfied. This section presents the data gathered for the three safety metrics with the experimental setup described in Ch. 8. The three safety metrics are the minimum distance at any given time during the execution of the path to a dynamic obstacle, the maximum cost along the path given by the cost distribution discussed in Eq. 6.5, and the average cost along the path.

Fig. 9.1 shows how the mean minimum distance changes as a function of the set speed of the robot and the amount of noise introduced to the trajectories of obstacles. The larger the minimum distance, the safer the path is. From the figure, it is evident that as the speed increases, so does the mean minimum distance Dodger. The amount of noise injected into the obstacle trajectories,  $\epsilon$ , does not seem to have any major effect on the minimum distance for any speed. For potential fields, as the speed increases, the increase in the minimum distance is not as drastic and the noise does not affect the overall safety given this metric. The differences between these two plots stem from the fact that a potential fields planner is purely reactive and Dodger generates a path by looking ahead. This means that the potential fields planner could move the robot through the path of an obstacle thus decreasing the minimum distance and increasing the possibility of a collision. Dodger will avoid moving the robot through the trajectory of an obstacle and thus is more likely to have a larger minimum distance along the path. For the gathered empirical data shown in Fig. 9.1, Dodger provided paths with a higher overall minimum distance than potential fields and as the speed of the robot increased, the minimum distance for the paths generated by Dodger out performed those generated by potential fields for this metric.

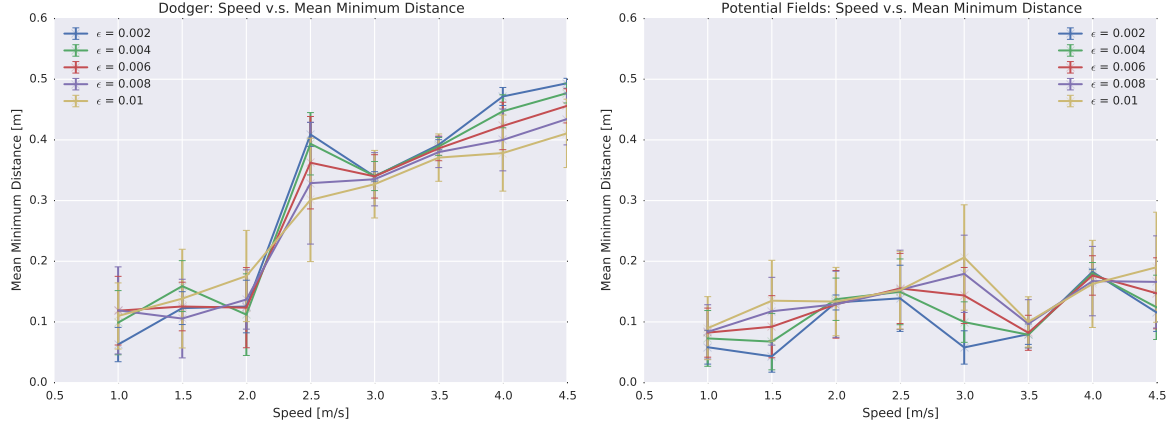


Figure 9.1: Plots showing how the minimum distance to any obstacle for a path changes as the speed increases for various amounts of obstacle position uncertainties. The horizontal axis represents the speed of the robot and the vertical axis represents the minimum distance to obstacles along the path. The different lines on each plot represent experiments with differing amounts of noise and the error bars represent one standard deviation. On the left is the graph for Dodger and on the right is the graph for the potential fields planner.

Fig. 9.2 shows how the maximum cost experienced along a path given by the cost distribution changes as a function of the set speed of the robot. The smaller the maximum cost, the safer the path. The figures shows that as the speed increases, the maximum cost experienced by a robot being planned using Dodger decreased. This is because when the robot is able to move faster, it can maneuver through areas that only have a low cost for a small period of time before becoming high cost areas again. Also, as the speed increased over  $2 \text{ m/s}$ , there was a greater difference between the maximum costs for paths through experimental configurations with small amounts of noise and the maximum costs for paths through high noise configurations. This is due to the fact that no matter how fast the robot is able to move, the more noise in a scene, the more the initial path will not represent the actual costs through the environment and the planner will need to replan. The robot may move to an area in which it thinks it will be safe, but if the obstacles deviate from their prescribed trajectories, this area may not be safe any longer and a new path is needed and therefore the cost for the path a robot is executing will increase. The paths generated by the potential fields planner did not have a similar behaviour as the amount of noise increased, however, the maximum cost was greater for all speeds than that of the paths generated by Dodger. This is because the potential fields planner does not take into account the trajectories of the obstacles when planning and is purely reactive. This plot shows that having access to information about where obstacles are moving can decrease the costs of the generated paths which in turn leads to safer trajectories for the robot.

Fig. 9.3 shows how the average cost along a path changes as the speed of the robot increases for Dodger and the potential fields planner. These plots are very similar to those in Fig. 9.2 however, there is an increase in the average cost for the potential fields. This is mostly likely because as the speed of the robot increases, the potential fields planner is able to move the robot through the path of an obstacle without being deviated or hit by the obstacle thus increasing the average cost along the path. Since the planner can move the robot through these areas quickly, instead of planning around the obstacle, the planner will just move quickly through the path of the obstacle. From these plots, it is evident that Dodger was able to generate paths with lower average costs than potential fields and as the speed of the robot increased, the average costs of the paths for Dodger decreased whereas the costs for paths generated by potential fields increased.

### 9.1.1 Variance

Representing the standard deviation as a function of the noise quantifies how consistent the planner is as the noise for a scene changes. The plots in Fig. 9.4 show how the standard deviation for the minimum distance metrics increases as the noise injected into the obstacle trajectory increases and the speed changes. The standard deviation for minimum distance metric increased more rapidly for Dodger than

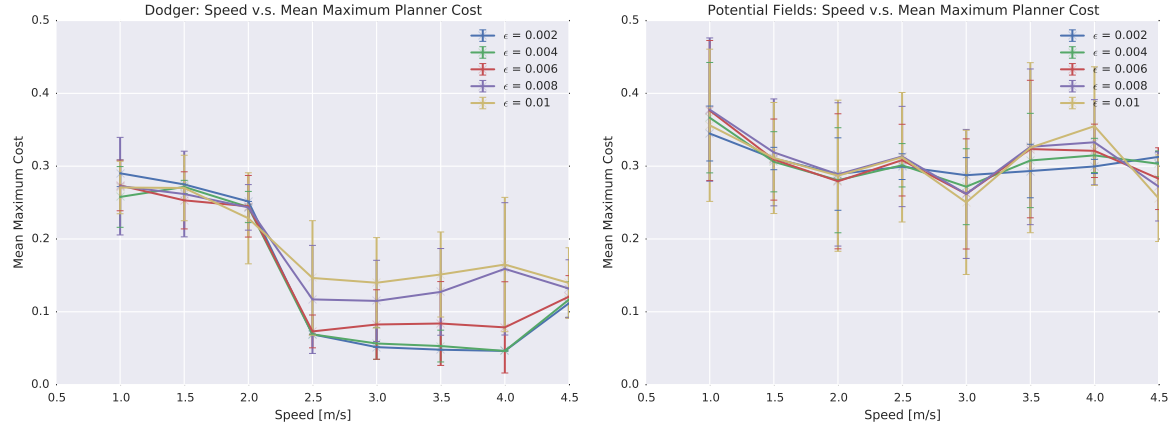


Figure 9.2: Plots showing how the maximum cost for a path changes as the speed increases for various amounts of obstacle position uncertainties. The horizontal axis represents the speed of the robot and the vertical axis represents the maximum cost along the path. The different lines on each plot represent experiments with differing amounts of noise and the error bars represent one standard deviation. On the left is the graph for Dodger and on the right is the graph for the potential fields planner.

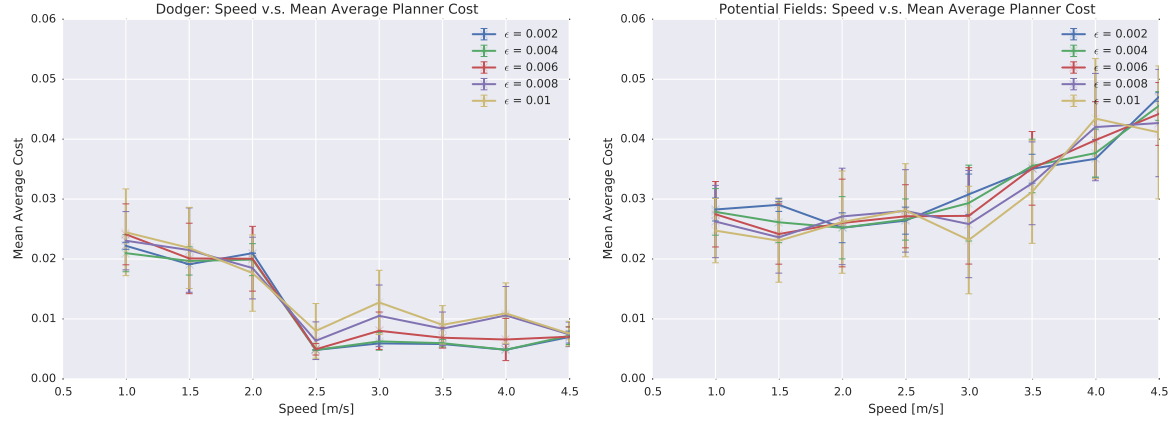


Figure 9.3: Plots showing how the average cost for a path changes as the speed increases for various amounts of obstacle position uncertainties. The horizontal axis represents the speed of the robot and the vertical axis represents the average cost along the path. The different lines on each plot represent experiments with differing amounts of noise and the error bars represent one standard deviation. On the left is the graph for Dodger and on the right is the graph for the potential fields planner.

for the potential fields planner. This is because there is a stochastic component in the planning for Dodger, the probabilistic roadmap. For some random generations of the roadmap, areas around where the obstacles are going to be are more heavily sampled, thus leading to greater variance in the results for the minimum distance. For the potential fields planner, there is no random component and is free to sample along the execution of its path and thus the standard deviation for this metric is only determined by the stochasticity of the dynamic obstacles and not by the algorithm.

The plots in Fig. 9.5 shows how the average and maximum costs change as the noise injected into the obstacle trajectories increases. The average and minimum costs for the paths generated by Dodger increases less rapidly than those generated by the potential fields planner. This is because Dodger is actively searching for low cost paths through the environment using the information about obstacle motion whereas the potential fields planner is just reacting the change in the potentials leading to the goal. Since the potential fields planner is not trying to minimize the cost of the generated path, there will be a larger variance in the average and maximum costs.

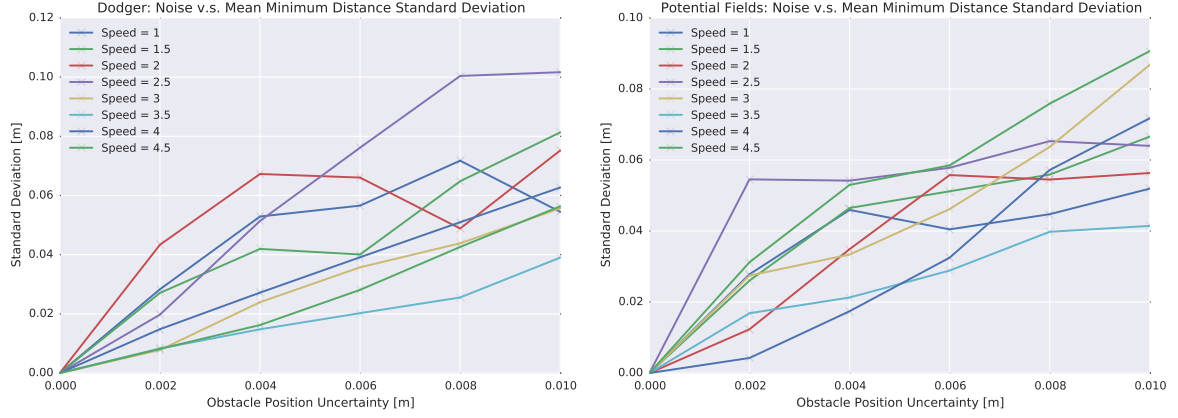


Figure 9.4: Plots showing how the standard deviation for the minimum distance along a path changes as the noise injected into the obstacle trajectories increases. The horizontal axis represents the amount of noise and the vertical axis represents the standard deviation. The different lines indicate different speeds that the robot was travelling. On the left is the graph for Dodger and on the right is the graph for the potential fields planner.

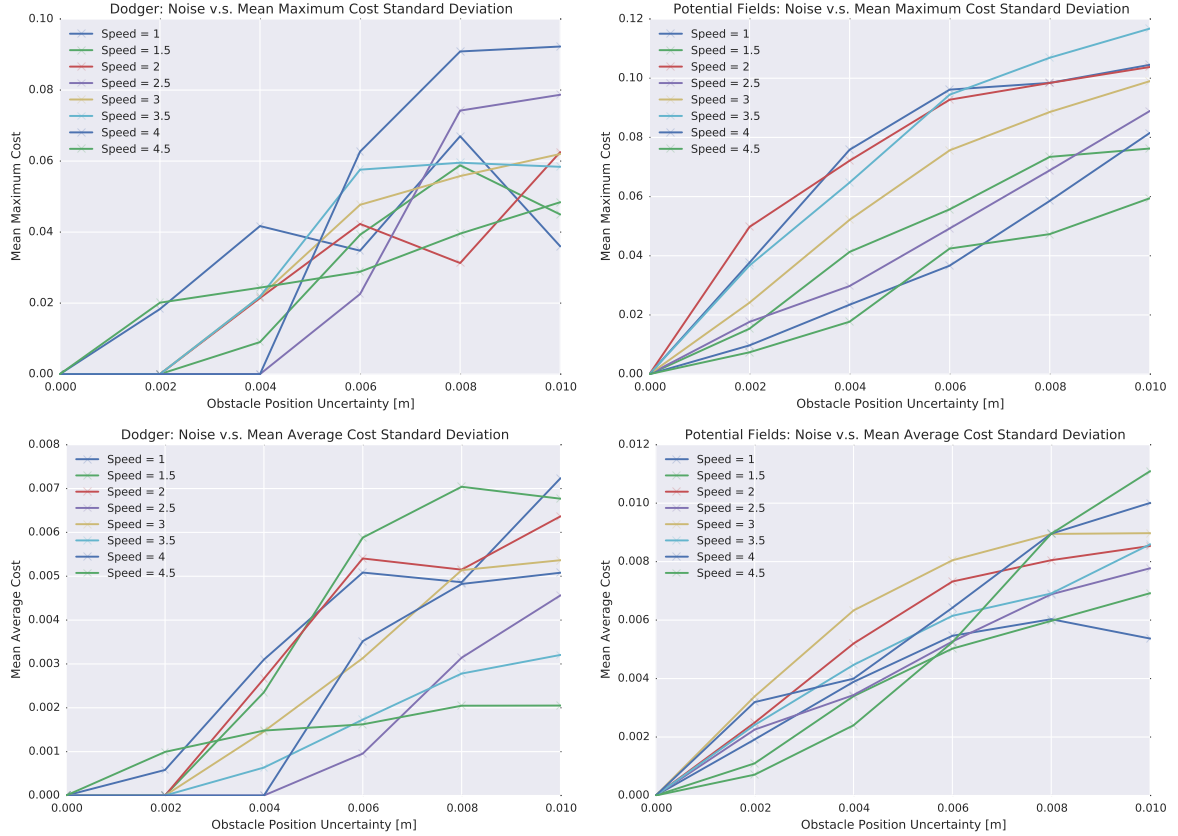


Figure 9.5: Plots showing how the standard deviation for the maximum cost and average cost along a path changes as the noise injected into the obstacle trajectories increases. The horizontal axis represents the amount of noise and the vertical axis represents the standard deviation. The different lines indicate different speeds that the robot was travelling. On the left is the graph for Dodger and on the right is the graph for the potential fields planner. The top row is for the maximum cost and the bottom row is for the average cost.

## 9.2 Computational Time

Showing how the computational time changes for different sets of parameters is useful to show how feasible the approach is in practice. For the two planners, the times it took to compute the paths were collected

and are shown in Fig. 9.6. The potential fields planner is able to find paths more quickly than Dodger and this is due to its purely reactive behaviour. Since the scenes used did not have any local minimas besides the goal, the potential fields planner is able to quickly find a path to the goal and as the speed increases, the amount of steps needed for it to search through the environment decreases thus decreasing the overall computational time. The computational time for Dodger also decreased as the speed increased, but the overall computational time was greater than potential fields. This is because Dodger uses a much more complex algorithm than potential fields requiring more computational time. For speeds less than  $2.5 \text{ m/s}$ , the time it takes Dodger to find a path may be infeasible for some situations. However, for speeds of  $2.5 \text{ m/s}$ , the computational time decreasing drastically making it feasible to use for real-time scenarios. Please note that computational times shown in Fig. 9.6 represent the overall time it takes the planner to find a path with replanning. This means that the planner is simultaneously executing and planning thus meaning that the robot reached the goal in at least the time presented in the figures.

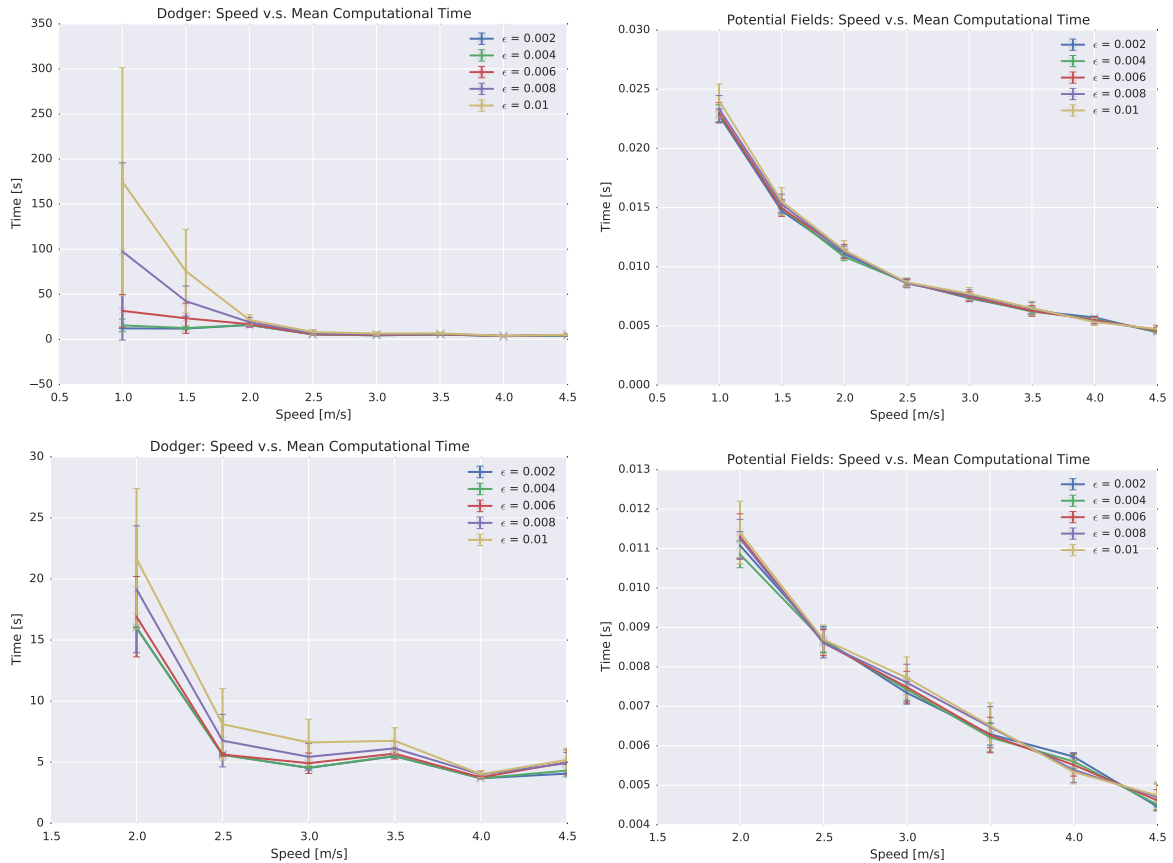


Figure 9.6: Plots showing how the computational time to generate a path changes as the speed increases for various amounts of obstacle position uncertainties. The horizontal axis represents the speed of the robot and the vertical axis represents the computational time to generate the path. The different lines on each plot represent experiments with differing amounts of noise and the error bars represent one standard deviation. On the left is the graph for Dodger and on the right is the graph for the potential fields planner.

### 9.2.1 Variance

As with the other metrics, seeing how the variance reacts to an increasing amount of noise is equally as important. Fig. 9.7 presents this relationship. The standard deviations for computational times for Dodger increase more rapidly than for the potential fields planner. This is because the Dodger had significantly larger computational times than the potential fields planner and would also have higher standard deviations. Likewise, the computational time standard deviations for Dodger are caused by both the randomness of the nodes used to create the probabilistic roadmap and the level of uncertainty injected into the obstacle trajectories. The standard deviation for the computational times for the

potential fields planner is only dependent on the amount of noise in the obstacles movements since the algorithm does not have any random components.

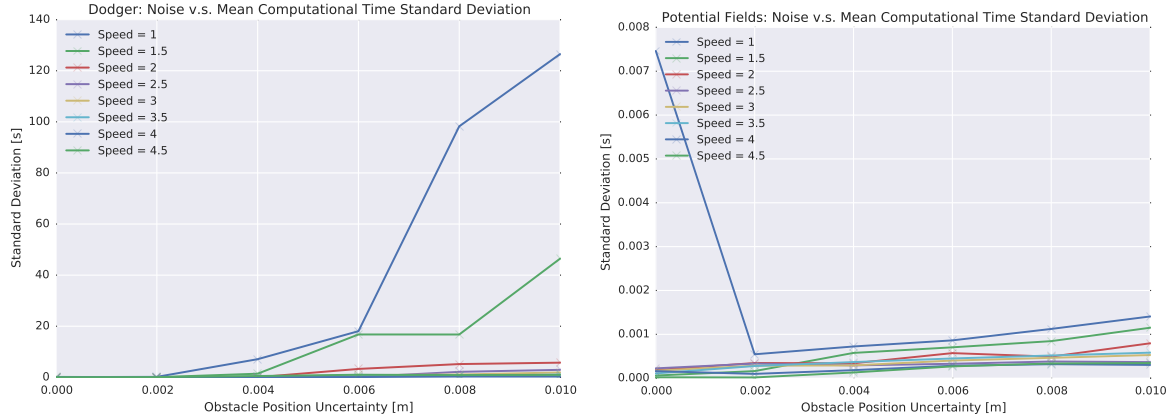


Figure 9.7: Plots showing how the standard deviation for the computational cost to generate a path changes as the noise injected into the obstacle trajectories increases. The horizontal axis represents the amount of noise and the vertical axis represents the standard deviation. The different lines indicate different speeds that the robot was travelling. On the left is the graph for Dodger and on the right is the graph for the potential fields planner.

### 9.3 Behaviour

Figures 9.8 and 9.9 show how Dodger and the potential fields planner respectively guide the robot through Scene 1 when the noise injected into the obstacle trajectories,  $\epsilon = 0.004$  and the speed,  $s = 1.5\text{m/s}$ . The robot is represented by the quadrotor, its path by the blue line, the obstacles by the mobile ground robots, and the initial and goal configurations by the red and green quadrotors respectively. Qualitatively, the paths generated by Dodger look safer than that of those generated by the potential fields planner. The potential fields planner even led the robot into collisions twice in the third and sixth snapshots in Fig. 9.9. This is because the obstacles are not within the sensing radius of the robot using potential fields until they are at their maximum velocity in the center of the scene and the robot is not able to move out of their way. Dodger generates a path that automatically moves the robot around the back of the oscillating obstacles such that it does not cross over their trajectories from side to side. This reduces the cost associated with the path and significantly reduces the chance that the robot will collide with an obstacle. Due to the stochasticity of the obstacles' movements, Dodger needed to replan more than once when executing the initial path. This occurred right before images three, four, and six. The path becomes jagged and changes direction quickly. This is because the original path is no longer safe because of the random movement of the obstacles.

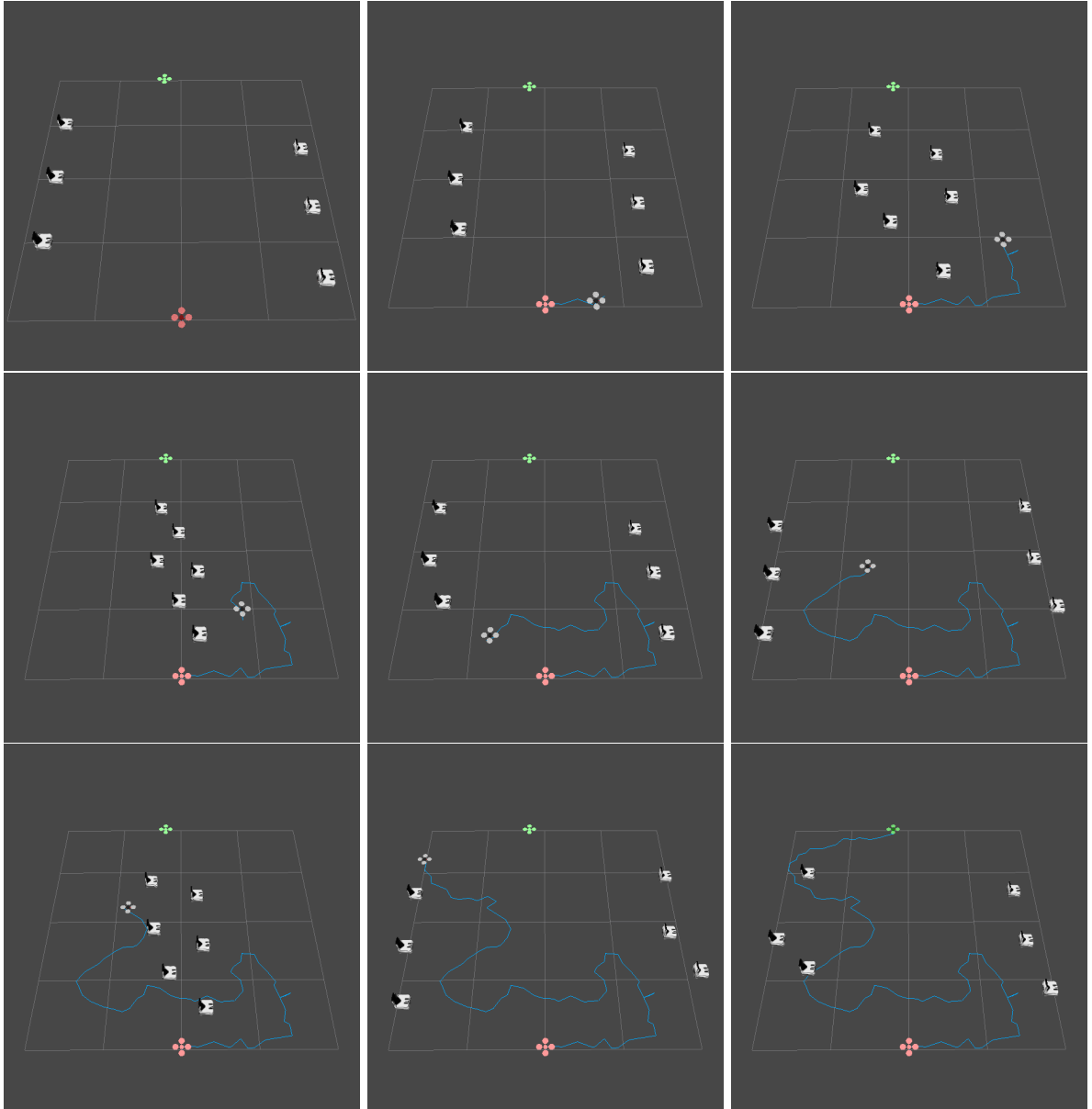


Figure 9.8: Images showing the progression of the robot, represented by the quadrotor, following a path generated by Dodger through Scene 1 from the initial configuration, represented by the red quadrotor shape, to the goal configuration, the green quadrotor shape. The obstacles are represented by the mobile ground robots and the path of the robot is shown by the blue line. The sequence of images progress from left to right, up to down.

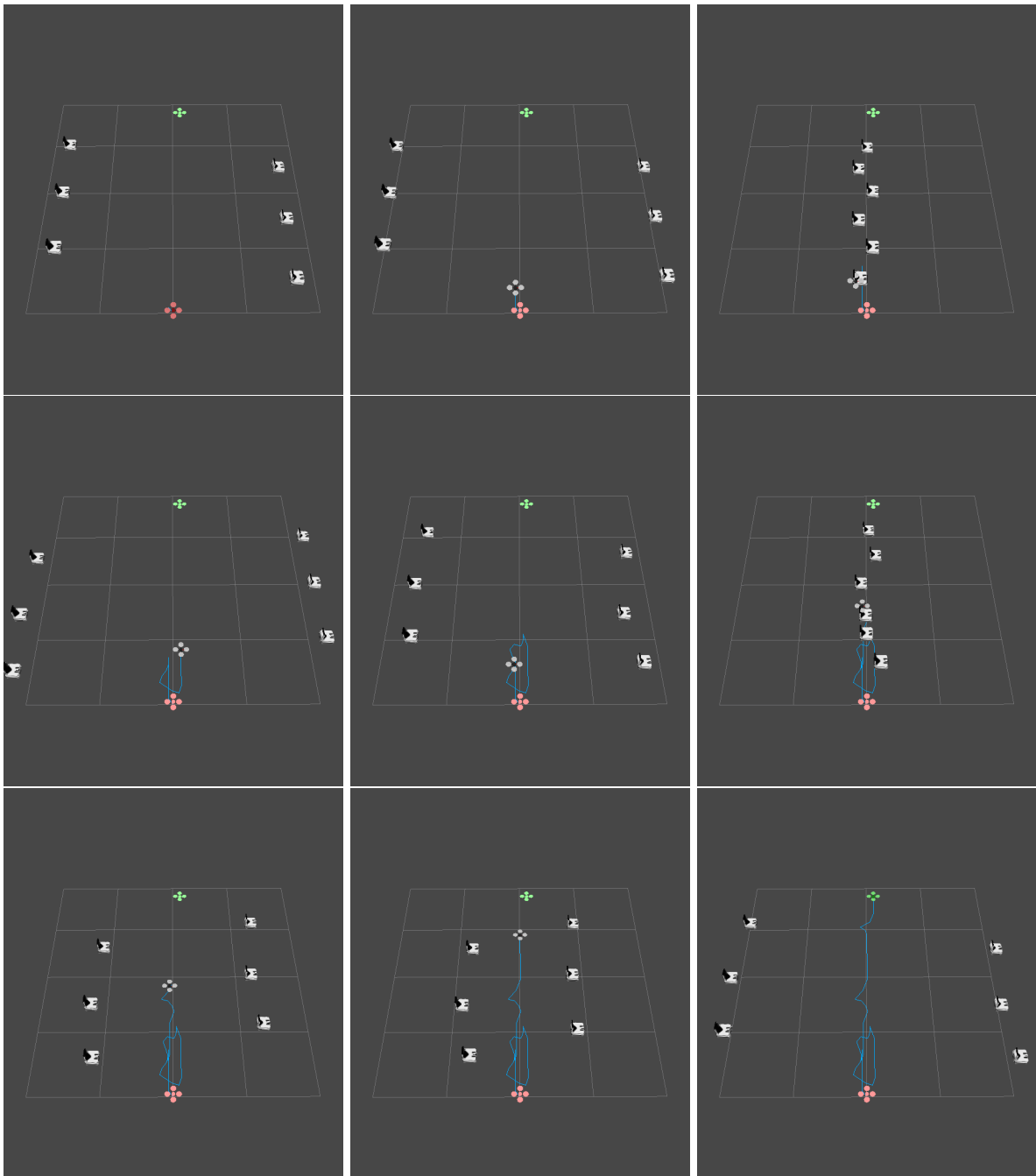


Figure 9.9: Images showing the progression of the robot, represented by the quadrotor, following a path generated by the potential fields planner through Scene 1 from the initial configuration, represented by the red quadrotor shape, to the goal configuration, the green quadrotor shape. The obstacles are represented by the mobile ground robots and the path of the robot is shown by the blue line. The sequence of images progress from left to right, up to down.

# CHAPTER 10

---

## Discussion

---

### 10.1 Future Work

There are many possible improvements to this project that could not be accomplished in the given time frame. This section addresses these future improvements and how they can impact the performance and robustness of the project.

#### 10.1.1 Pruning the Search Tree

Currently, the only mechanism used to prune the search tree is the priority of the nodes being expanded. This allows some nodes in the probabilistic roadmap not to be expanded thus limiting the overall size of the tree. However, more complex machine learning techniques could be used such as limiting the density of the search tree in certain areas and not expanding nodes in a geometric area that have consistently shown to have higher costs. Pruning the search tree could have drastic result in reducing the computational time needed to find a safe path because less nodes would need to be expanded and searched. Another approach at limiting the size of the search tree could be to use another heuristic that could provide some information about how close a certain node is to reaching the goal. This would find paths to the goal more quickly because the search is more directed. There would have to be some constraints used in this heuristic, for instance, its influence in the priority of a node in the queue because the safeness of a path would be sacrificed in return for decreased computational time. Likewise, decreasing the average degree of a node in the probabilistic roadmap whilst ensuring that the probabilistic roadmap is one connected component would limit the size of the search tree and thus the computational time. This could be done by using alternative roadmap construction methods such as connecting the  $k$ -nearest neighbours instead of all nodes within a given radius.

#### 10.1.2 Variable Speed and Wait Time

There are two constants in this work, the speed and wait time, which if made dynamic would increase the robustness of the algorithm. It is assumed that the robot will travel at a constant speed at all times unless it is waiting for a set period of time. However, there may be some reasons for increasing or decreasing the speed of the robot during runtime. For instance, if the robot were to also try and save energy, it may not to maintain a high speed, but only increase its speed when it is needed to

avoid coming into contact with obstacles in order to improve safety and minimize energy usage. Also, determining dynamically how long the robot should wait at a given location instead of having a set length of time would increase the robustness of the approach. By using a constant wait time, it is assumed that that interval is the best possible amount of time to stay stationary. In reality, in some situations, the robot will need to wait for longer than others. This is currently not incorporated into the approach and would be a valuable addition.

### 10.1.3 Increasing Robot Dimensionality

In the current work, it is assumed that the robot is a two dimensional point in space. This means that the robot occupies at any given time a certain point in space and that point in space exclusively. Many robot systems operate in higher dimensional spaces such as snake robots and unmanned aerial vehicles. Snake robots operate in the same dimension as the number of links it has. Unmanned aerial vehicles operate in three dimensional space because they are able to fly. By incorporating higher dimensional vehicle models into the algorithm, paths for more classes of robots can be generated and thus makes the approach more robust.

### 10.1.4 Real World Experiments

Since this project is concerned with moving a physical robot through an environment, an important piece of future work would be to conduct experiments using a physical robot in a real-world scenario. This would mean adapting the path generated for the robot into a list of control inputs that would account for the physics of the robot to move it to the goal. Since the project provides a sequence of spatio-temporal waypoints, a specialized controller can be created for different mobile robots that could follow the waypoints generated. It may also be beneficial to utilize the control model for the given robot into the planning. So instead of the result of the planning algorithm returning a sequence of waypoints, it could directly return a sequence of control inputs that could be fed into a robot's controller to move it to the goal. Another important component of implementing the system on a mobile robot would be the active prediction of obstacle movements. In this work, it is assumed that there is an external system being used that can determine where obstacles are going to move in the future. This system would either have to be implemented or an existing one used in order for the algorithm to work in real-time. This motion prediction system could either be its own component in an open loop system (like those found in warehouses), or the motion prediction could occur directly on the robot. If it is the latter, novel algorithms are going to need to be developed that are able to predict the motion of obstacles relatively quickly due to the limits set by the robot's processing power.

### 10.1.5 More Complex Models of Obstacle Behaviour

Obstacle behaviour in the current work is very simple. Obstacles are assumed to move along their prescribed trajectory with a set amount of uncertainty and are not affected by the actions of the robot or the other obstacles near it. It is also assumed that the obstacles will only follow one trajectory function and the current formulation does not account for obstacles with dynamic trajectory equations. The goal of future work would be to formalize a more complete model of the way an obstacle moves through the environment by incorporating reactive behaviour and multiple trajectory equations with associated spatio-temporal probabilities of switching between them. The reactive behaviour will encompass how the obstacle will react when other objects, either other obstacles or the robot being planned, move toward the obstacle or interfere with its trajectory. Likewise, the obstacles can be assumed to also be autonomous agents with their own planning algorithm. Accounting for this behaviour will result in a more comprehensive and realistic model of dynamic obstacles.

### 10.1.6 Multi-robot Coordination

Another extension to the current algorithms provided in this work would be to allow them to plan for multiple robots simultaneously. The current implementation only provides a path through a stochastic dynamic environment for a single robot. Many applications of robotics need multiple robots to move through the environment safely and at the same time. These algorithms are usually called swarming algorithms. By extending the current algorithms to find the  $k$ -safest paths through the environment in space-time, paths can be generated for multiple robots and thus safely plan the movements of a swarm to its goal.

## 10.2 Evaluation & Conclusion

From the results of the experiments shown in Ch. 9, it is evident that the algorithms proposed in this work are able to generate quantitatively and qualitatively safer paths than potential fields, a standard approach at planning through stochastic dynamic environments. As the speed increased, the paths generated by Dodger had higher minimum distances to obstacles and lower maximum and average costs along the path. This means that Dodger could generate paths that stayed farther away from obstacles than potential fields. Also, since it has information about where the obstacles are moving, the cost incurred by the robot along the paths generated by Dodger were lower than those generated by the potential fields planner. The paths did take longer to compute by Dodger than the potential fields planner, but the times were reasonable enough to use a real-time scenario. As computers become smaller and their processing power increases, the computational time needed to generate a path will decrease. For both planners and all metrics, the standard deviations increased at roughly the same rate as the noise injected into the trajectories of the obstacles increased. This is because the variance in the results are highly dependent on the motions of the obstacles. The more uncertainty in the obstacle trajectories, the more each planner will have to adjust its plan to cope.

From the metrics described in Ch. 8 Dodger is able to outperform a standard approach for planning in stochastic dynamic environments. The algorithms developed are able to leverage the information available about the motions of obstacles in order to guide a robot along safe, low cost paths from an initial configuration to a goal configuration. Dodger is also able to actively generate new paths in real-time to the goal configuration if it senses that the obstacles have deviated too far from their prescribed trajectories. This replanning enables the robot to react to the stochasticity and uncertainty of the environment and maintain a safe trajectory to the goal. The novel representation of dynamic obstacles and the algorithms used to plan around them shed light on a new way of path planning that can make use of available information from the environment to keep the robot and more importantly, the agents acting in the environment (i.e. humans, cars, other robots, etc) safe.

# CHAPTER 11

---

## Ethics

---

Since this project does not use any personal or classified information and the algorithms developed have not been tested with humans as obstacles, this project does not raise any ethical concerns. One could argue that the algorithms developed could be used in the robot uprising, but that is not the intention of the work and the robot uprising is not set to come for another few decades. A possible vessel for this uprising is shown in Fig. 11.1 [42].



Figure 11.1: A picture of a possible vessel for the robot uprising

---

## Appendix

---

This appendix contains plots from the experiments conducted on Scenes 2 and 3. Note that for Scene 2, the potential fields planner was not able to complete find a path to the goal on sufficiently many cases and thus results could not be concluded. This is a consequence of using a potential fields planner, it may not bring the robot to the goal if it gets stuck in a local minima.

---

## Appendix I Results for Scene 2

---

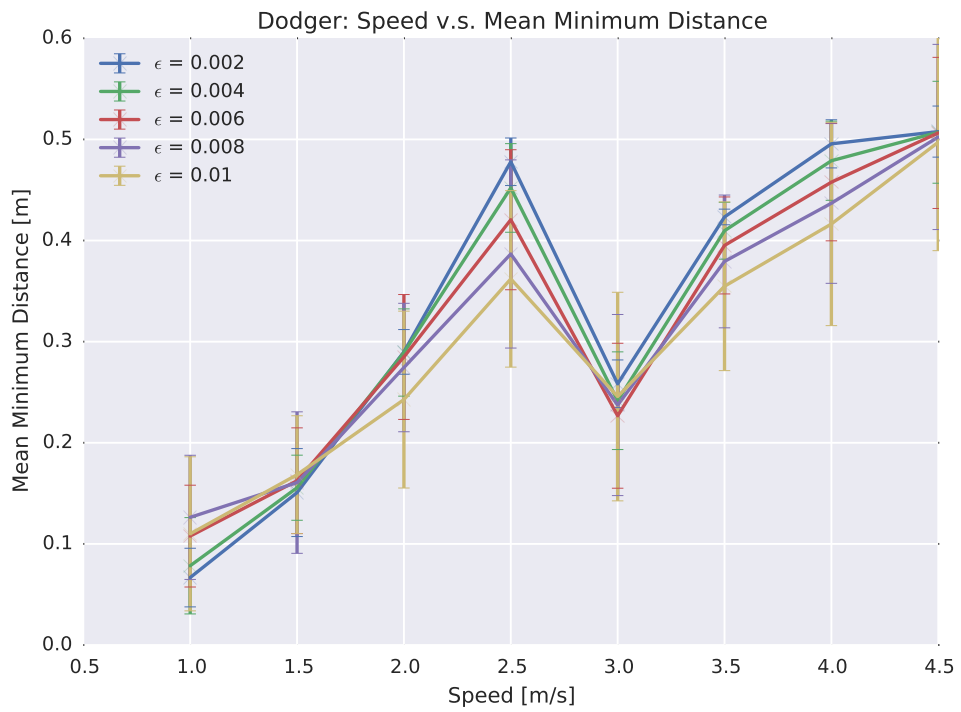


Figure 11.2: Plots showing how the minimum distance to any obstacle for a path changes as the speed increases for various amounts of obstacle position uncertainties. The horizontal axis represents the speed of the robot and the vertical axis represents the minimum distance to obstacles along the path. The different lines on each plot represent experiments with differing amounts of noise and the error bars represent one standard deviation.

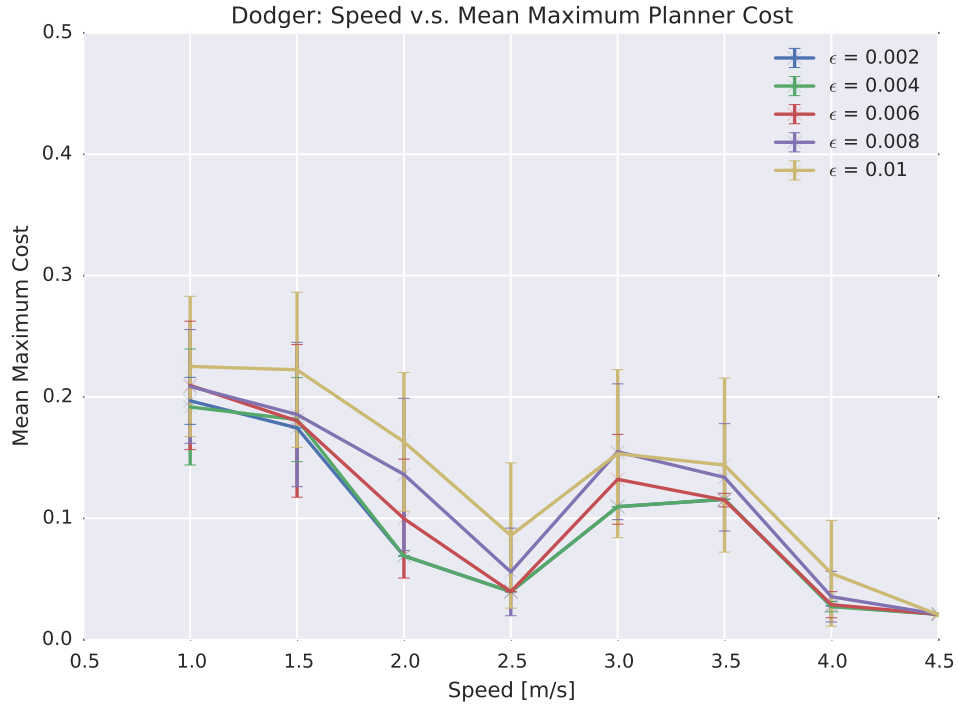


Figure 11.3: Plots showing how the maximum cost for a path changes as the speed increases for various amounts of obstacle position uncertainties. The horizontal axis represents the speed of the robot and the vertical axis represents the maximum cost along the path. The different lines on each plot represent experiments with differing amounts of noise and the error bars represent one standard deviation.

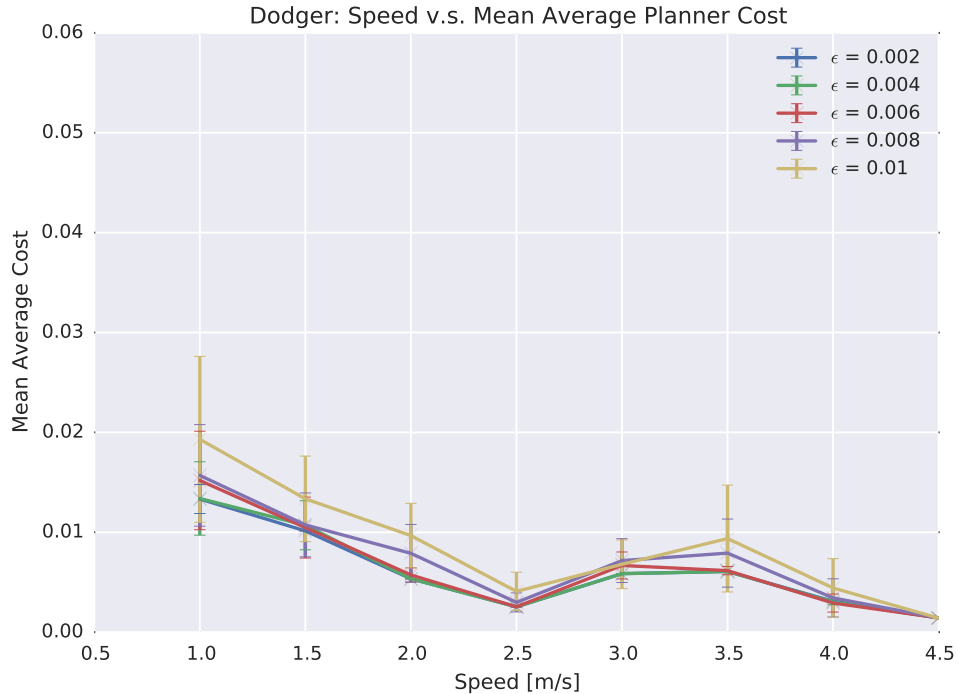


Figure 11.4: Plots showing how the average cost for a path changes as the speed increases for various amounts of obstacle position uncertainties. The horizontal axis represents the speed of the robot and the vertical axis represents the average cost along the path. The different lines on each plot represent experiments with differing amounts of noise and the error bars represent one standard deviation.

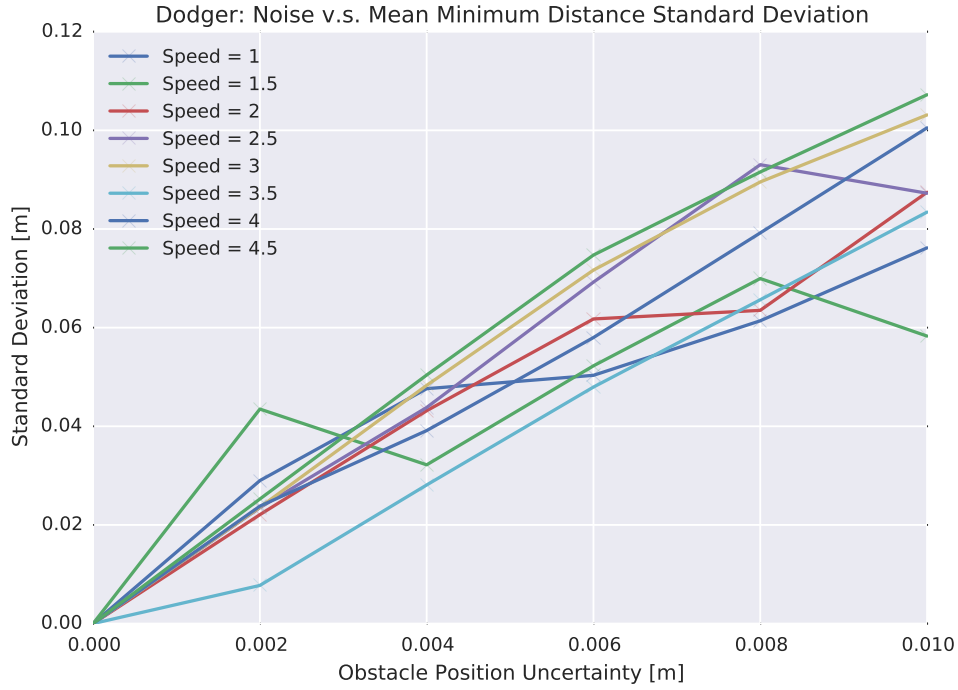


Figure 11.5: Plots showing how the standard deviation for the minimum distance along a path changes as the noise injected into the obstacle trajectories increases. The horizontal axis represents the amount of noise and the vertical axis represents the standard deviation. The different lines indicate different speeds that the robot was travelling.

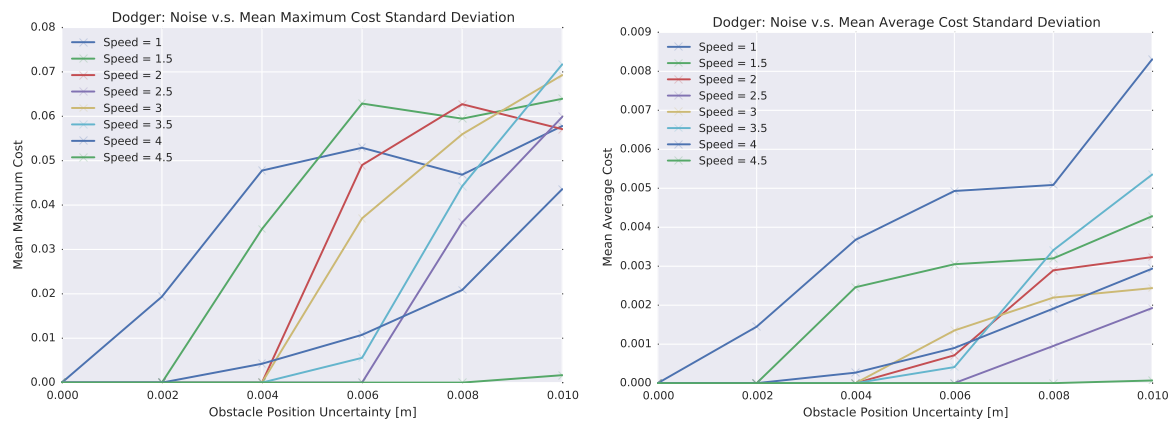


Figure 11.6: Plots showing how the standard deviation for the maximum cost and average cost along a path changes as the noise injected into the obstacle trajectories increases. The horizontal axis represents the amount of noise and the vertical axis represents the standard deviation. The different lines indicate different speeds that the robot was travelling. On the left is the graph for Dodger and on the right is the graph for the potential fields planner.

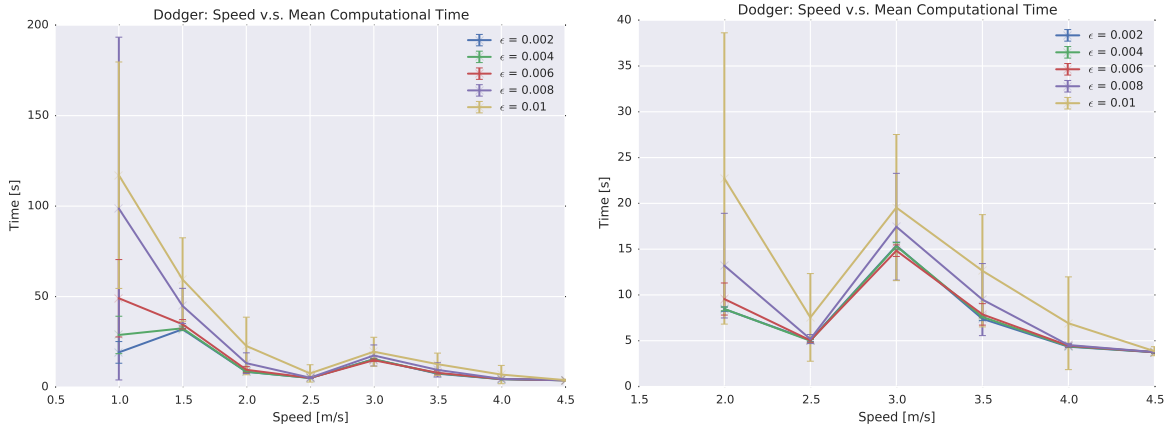


Figure 11.7: Plots showing how the computational to generate a path changes as the speed increases for various amounts of obstacle position uncertainties. The horizontal axis represents the speed of the robot and the vertical axis represents the computational time to generate the path. The different lines on each plot represent experiments with differing amounts of noise and the error bars represent one standard deviation.

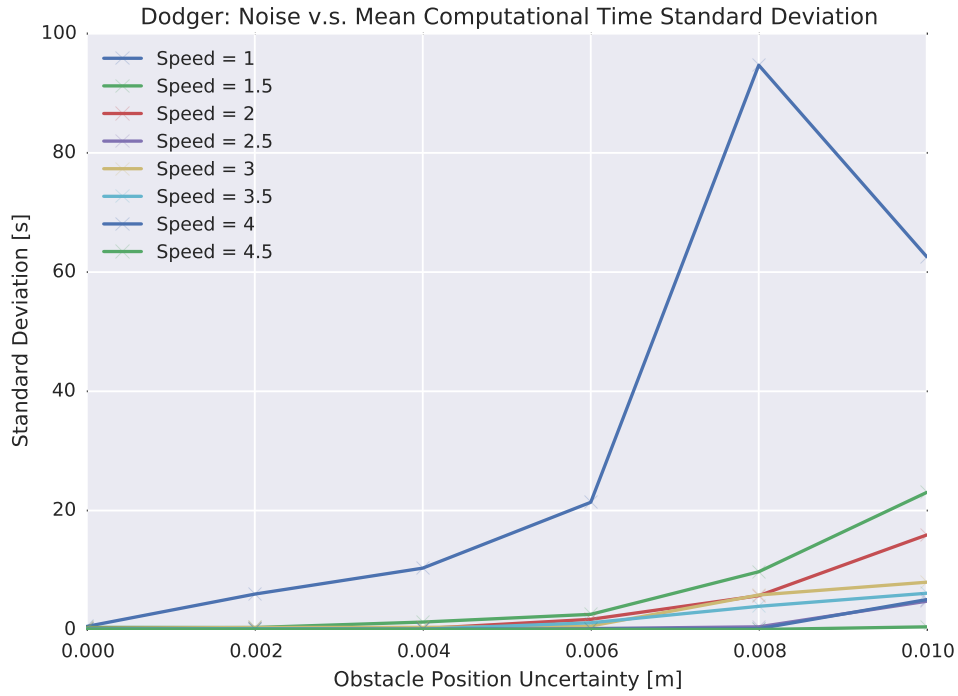


Figure 11.8: Plots showing how the standard deviation for the computational cost to generate a path changes as the noise injected into the obstacle trajectories increases. The horizontal axis represents the amount of noise and the vertical axis represents the standard deviation. The different lines indicate different speeds that the robot was travelling.

---

## Appendix II

### Results for Scene 3

---

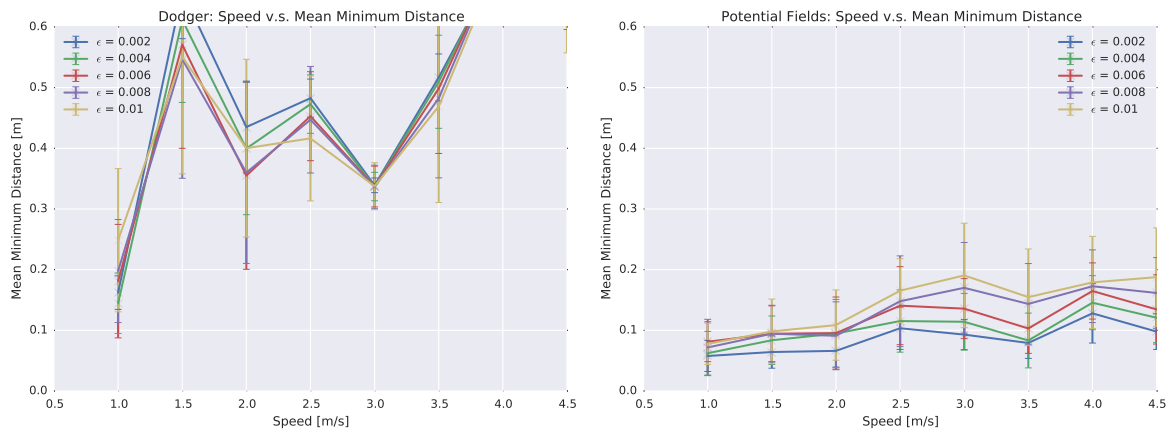


Figure 11.9: Plots showing how the minimum distance to any obstacle for a path changes as the speed increases for various amounts of obstacle position uncertainties. The horizontal axis represents the speed of the robot and the vertical axis represents the minimum distance to obstacles along the path. The different lines on each plot represent experiments with differing amounts of noise and the error bars represent one standard deviation. On the left is the graph for Dodger and on the right is the graph for the potential fields planner.

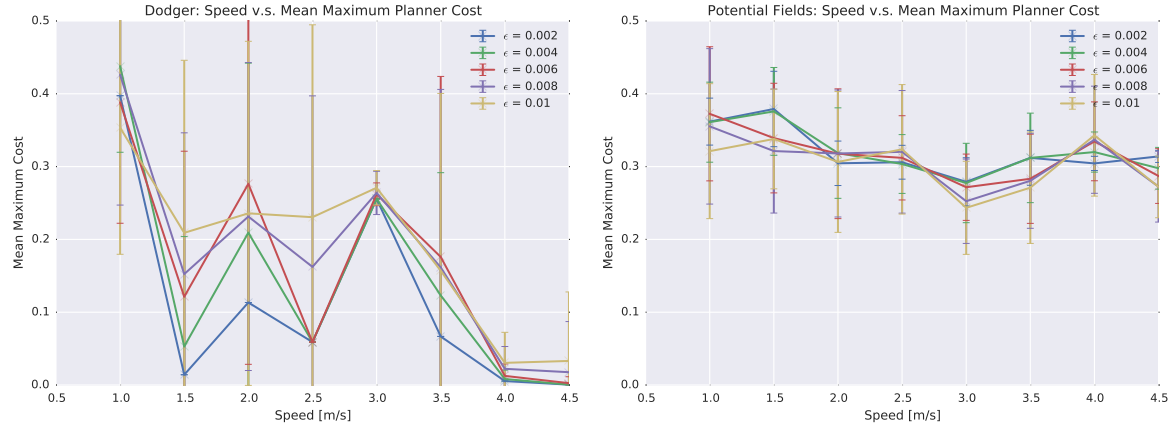


Figure 11.10: Plots showing how the maximum cost for a path changes as the speed increases for various amounts of obstacle position uncertainties. The horizontal axis represents the speed of the robot and the vertical axis represents the maximum cost along the path. The different lines on each plot represent experiments with differing amounts of noise and the error bars represent one standard deviation. On the left is the graph for Dodger and on the right is the graph for the potential fields planner.

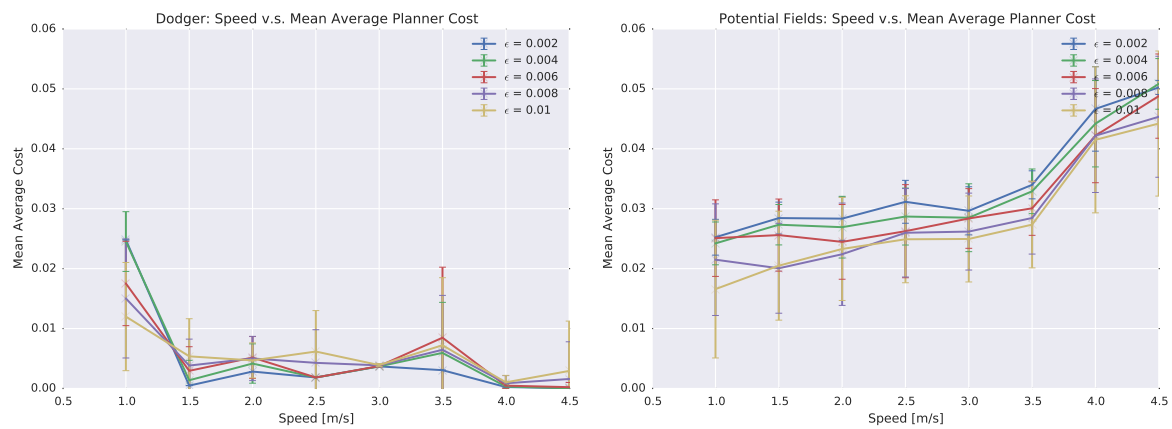


Figure 11.11: Plots showing how the average cost for a path changes as the speed increases for various amounts of obstacle position uncertainties. The horizontal axis represents the speed of the robot and the vertical axis represents the average cost along the path. The different lines on each plot represent experiments with differing amounts of noise and the error bars represent one standard deviation. On the left is the graph for Dodger and on the right is the graph for the potential fields planner.

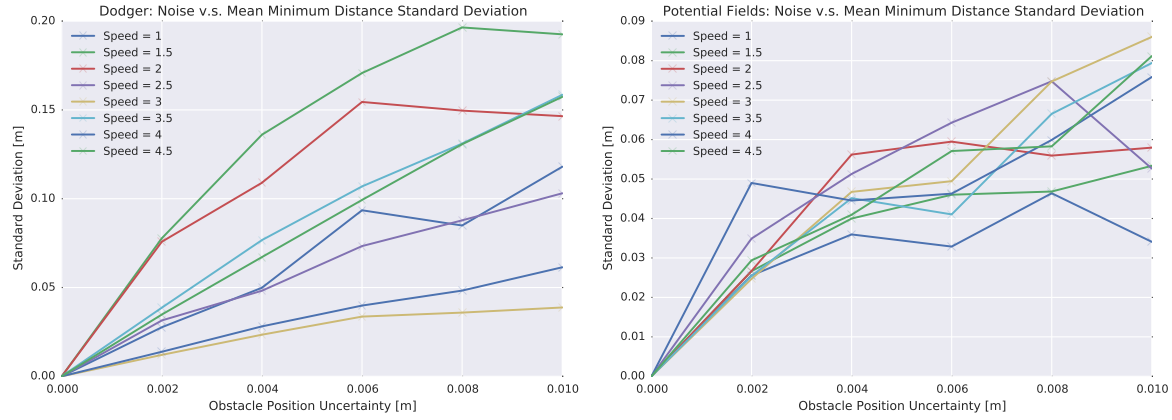


Figure 11.12: Plots showing how the standard deviation for the minimum distance along a path changes as the noise injected into the obstacle trajectories increases. The horizontal axis represents the amount of noise and the vertical axis represents the standard deviation. The different lines indicate different speeds that the robot was travelling. On the left is the graph for Dodger and on the right is the graph for the potential fields planner.

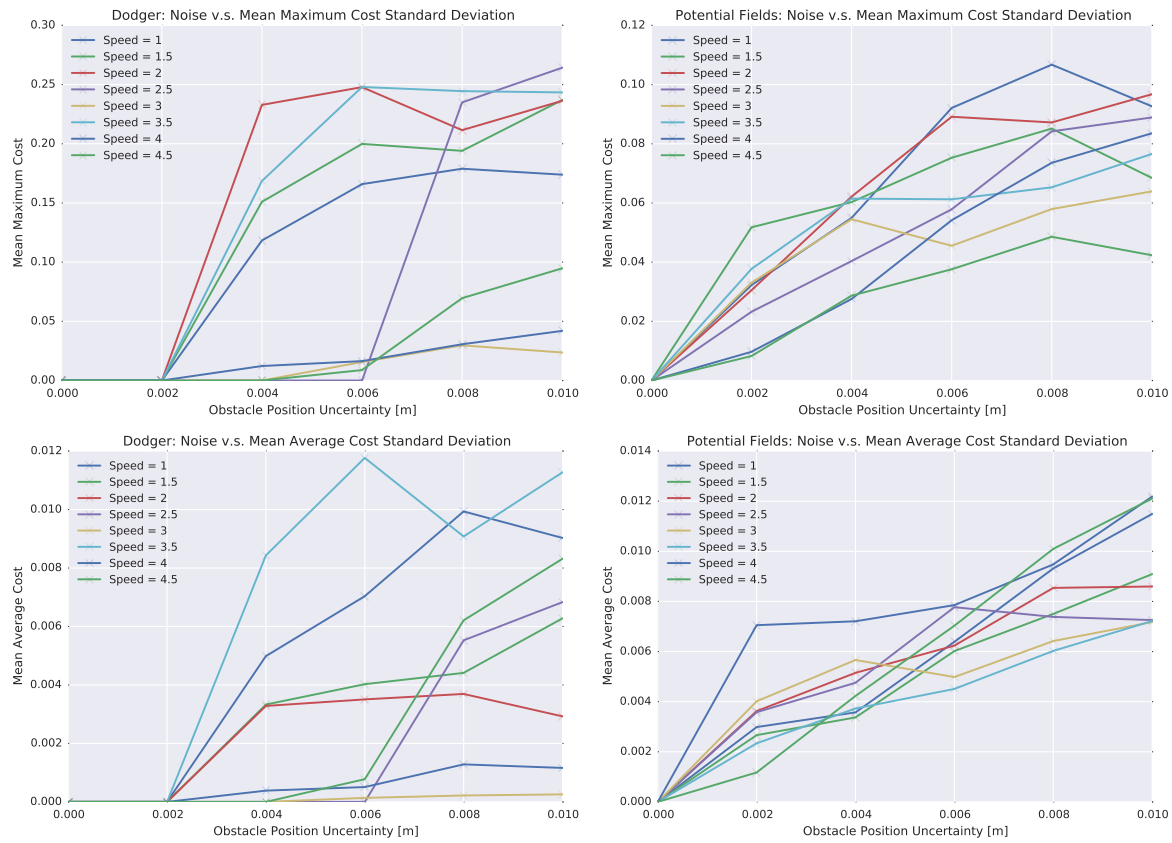


Figure 11.13: Plots showing how the standard deviation for the maximum cost and average cost along a path changes as the noise injected into the obstacle trajectories increases. The horizontal axis represents the amount of noise and the vertical axis represents the standard deviation. The different lines indicate different speeds that the robot was travelling. On the left is the graph for Dodger and on the right is the graph for the potential fields planner. The top row is for the maximum cost and the bottom row is the for the average cost.

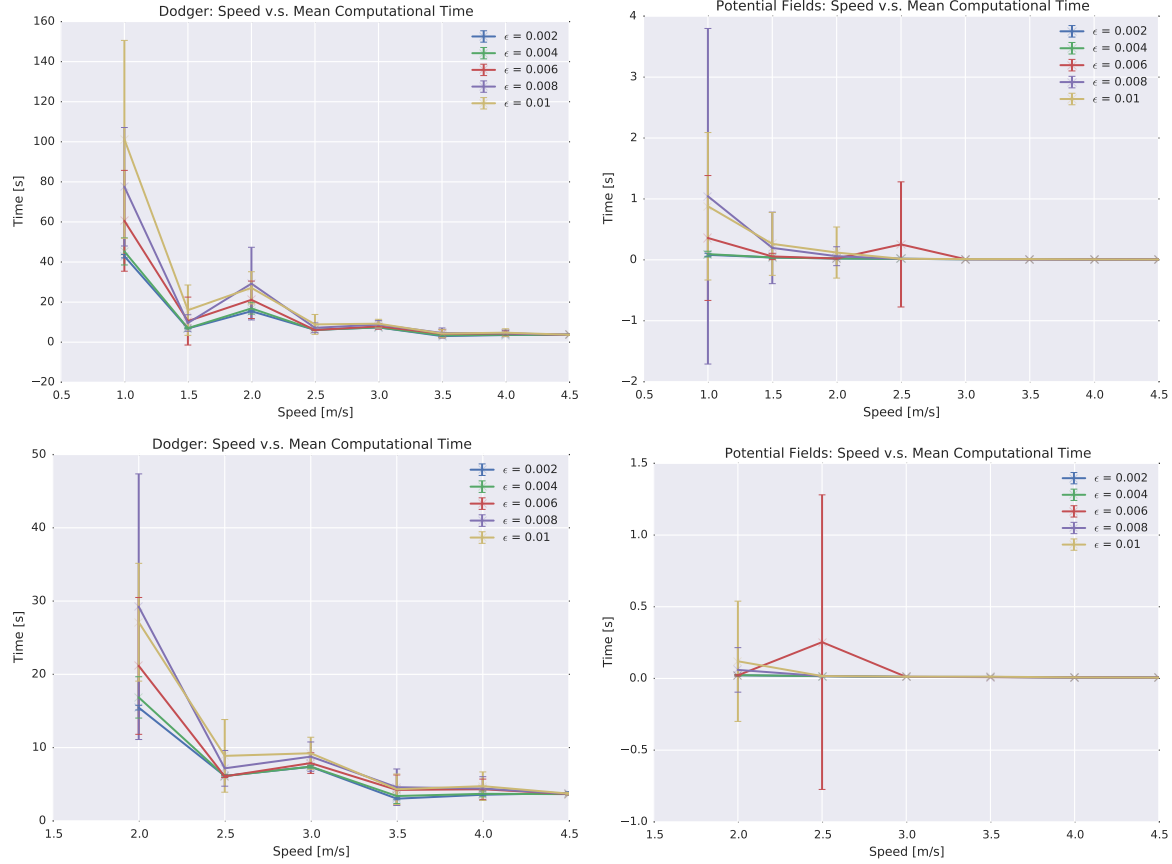


Figure 11.14: Plots showing how the computational time to generate a path changes as the speed increases for various amounts of obstacle position uncertainties. The horizontal axis represents the speed of the robot and the vertical axis represents the computational time to generate the path. The different lines on each plot represent experiments with differing amounts of noise and the error bars represent one standard deviation. On the left is the graph for Dodger and on the right is the graph for the potential fields planner.

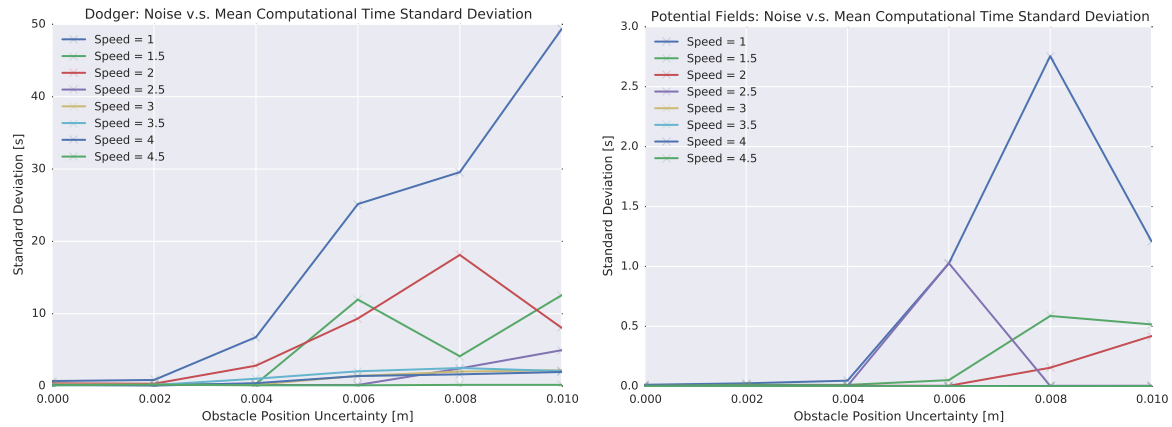


Figure 11.15: Plots showing how the standard deviation for the computational cost to generate a path changes as the noise injected into the obstacle trajectories increases. The horizontal axis represents the amount of noise and the vertical axis represents the standard deviation. The different lines indicate different speeds that the robot was travelling. On the left is the graph for Dodger and on the right is the graph for the potential fields planner.

---

## Bibliography

---

- [1] H. M. Choset, *Principles of robot motion: theory, algorithms, and implementation*. MIT press, 2005.
- [2] S. M. LaValle, *Planning algorithms*. Cambridge university press, 2006.
- [3] M. Weir, A. Buck, and J. Lewis, “Potbug: A minds eye approach to providing bug-like guarantees for adaptive obstacle navigation using dynamic potential fields,” in *From Animals to Animats 9* (S. Nolfi, G. Baldassarre, R. Calabretta, J. Hallam, D. Marocco, J.-A. Meyer, O. Miglino, and D. Parisi, eds.), vol. 4095 of *Lecture Notes in Computer Science*, pp. 239–250, Springer Berlin Heidelberg, 2006.
- [4] T. Lozano-Pérez and M. A. Wesley, “An algorithm for planning collision-free paths among polyhedral obstacles,” *Commun. ACM*, vol. 22, pp. 560–570, Oct. 1979.
- [5] J. E. Galletly, “An overview of genetic algorithms,” *Kybernetes*, vol. 21, no. 6, pp. 26–30, 1992.
- [6] Y. Wang, I. P. Sillitoe, and D. J. Mulvaney, “Mobile robot path planning in dynamic environments,” in *Robotics and Automation, 2007 IEEE International Conference on*, pp. 71–76, IEEE, 2007.
- [7] A. Zhou, B.-Y. Qu, H. Li, S.-Z. Zhao, P. N. Suganthan, and Q. Zhang, “Multiobjective evolutionary algorithms: A survey of the state of the art,” *Swarm and Evolutionary Computation*, vol. 1, no. 1, pp. 32 – 49, 2011.
- [8] R. Smierzchalski and Z. Michalewicz, “Path planning in dynamic environments,” in *Innovations in Robot Mobility and Control*, pp. 135–153, Springer, 2005.
- [9] J. Kennedy, “Particle swarm optimization,” in *Encyclopedia of Machine Learning*, pp. 760–766, Springer, 2010.
- [10] G. Dunwei and G. Na, “Local robot path planning with predicting band trajectories of obstacles,” in *Natural Computation (ICNC), 2011 Seventh International Conference on*, vol. 3, pp. 1734–1738, IEEE, 2011.
- [11] V. Narayanan, M. Phillips, and M. Likhachev, “Anytime safe interval path planning for dynamic environments,” in *Intelligent Robots and Systems (IROS), 2012 IEEE/RSJ International Conference on*, pp. 4708–4715, IEEE, 2012.
- [12] M. Phillips and M. Likhachev, “Sipp: Safe interval path planning for dynamic environments,” in *Robotics and Automation (ICRA), 2011 IEEE International Conference on*, pp. 5628–5635, IEEE, 2011.
- [13] M. Likhachev, G. J. Gordon, and S. Thrun, “Ara\*: Anytime a\* with provable bounds on sub-optimality,” in *Advances in Neural Information Processing Systems*, p. None, 2003.

- [14] J. Van Den Berg, D. Ferguson, and J. Kuffner, "Anytime path planning and replanning in dynamic environments," in *Robotics and Automation, 2006. ICRA 2006. Proceedings 2006 IEEE International Conference on*, pp. 2366–2371, IEEE, 2006.
- [15] S. Koenig and M. Likhachev, "D\* lite.," in *AAAI/IAAI*, pp. 476–483, 2002.
- [16] D. Hsu, R. Kindel, J.-C. Latombe, and S. Rock, "Randomized kinodynamic motion planning with moving obstacles," *The International Journal of Robotics Research*, vol. 21, no. 3, pp. 233–255, 2002.
- [17] B. Jensen, R. Philippse, and R. Siegwart, "Motion detection and path planning in dynamic environments," in *Workshop Proceedings Reasoning with Uncertainty in Robotics, International Joint Conference on Artificial Intelligence (IJCAI)*, 2003.
- [18] S. Rodriguez, J.-M. Lien, and N. M. Amato, "A framework for planning motion in environments with moving obstacles," in *Intelligent Robots and Systems, 2007. IROS 2007. IEEE/RSJ International Conference on*, pp. 3309–3314, IEEE, 2007.
- [19] S. M. LaValle, "Rapidly-exploring random trees a new tool for path planning," 1998.
- [20] Y. Koren and J. Borenstein, "Potential field methods and their inherent limitations for mobile robot navigation," in *Robotics and Automation, 1991. Proceedings., 1991 IEEE International Conference on*, pp. 1398–1404, IEEE, 1991.
- [21] A. Wallar and E. Plaku, "Path planning for swarms by combining probabilistic roadmaps and potential fields," in *Towards Autonomous Robotic Systems*, pp. 417–428, Springer, 2014.
- [22] A. Wallar and E. Plaku, "Path planning for swarms in dynamic environments by combining probabilistic roadmaps and potential fields," in *Swarm Intelligence (SIS), 2014 IEEE Symposium on*, pp. 1–8, IEEE, 2014.
- [23] L. Kavraki, P. Svestka, J.-C. Latombe, and M. Overmars, "Probabilistic roadmaps for path planning in high-dimensional configuration spaces," *Robotics and Automation, IEEE Transactions on*, vol. 12, pp. 566–580, Aug 1996.
- [24] G. Alankus, N. Atay, C. Lu, and O. Bayazit, "Spatiotemporal query strategies for navigation in dynamic sensor network environments," in *Intelligent Robots and Systems, 2005. (IROS 2005). 2005 IEEE/RSJ International Conference on*, pp. 3718–3725, Aug 2005.
- [25] P. Hart, N. Nilsson, and B. Raphael, "A formal basis for the heuristic determination of minimum cost paths," *Systems Science and Cybernetics, IEEE Transactions on*, vol. 4, pp. 100–107, July 1968.
- [26] E. Dijkstra, "A note on two problems in connexion with graphs," *Numerische Mathematik*, vol. 1, no. 1, pp. 269–271, 1959.
- [27] J. Edmonds, "Optimum branching," *Journal OF Research of the National Bureau of Standards*, November 1967.
- [28] J. B. Kruskal, "On the shortest spanning subtree of a graph and the traveling salesman problem," *Proceedings of the American Mathematical Society*, vol. 7, p. 4850, 1956.
- [29] R. C. Prim, "Shortest connection networks and some generalizations," *Bell System Technical Journal*, vol. 36, p. 13891401, 1957.
- [30] J. M. Phillips, N. Bedrossian, and E. Kavraki, "Guided expansive spaces trees: A search strategy for motion-and cost-constrained state spaces," in *Robotics and Automation, 2004. Proceedings. ICRA '04. 2004 IEEE International Conference on*, vol. 4, pp. 3968–3973, IEEE, 2004.
- [31] R. E. Korf, "Linear-space best-first search," *Artificial Intelligence*, vol. 62, no. 1, pp. 41–78, 1993.
- [32] C. Sung, D. Feldman, and D. Rus, "Trajectory clustering for motion prediction," in *Intelligent Robots and Systems (IROS), 2012 IEEE/RSJ International Conference on*, pp. 1547–1552, Oct 2012.
- [33] P. P. Choi and M. Hebert, "Learning and predicting moving object trajectory: a piecewise trajectory segment approach," *Robotics Institute*, p. 337, 2006.

## BIBLIOGRAPHY

---

- [34] T. Liu, P. Bahl, and I. Chlamtac, “Mobility modeling, location tracking, and trajectory prediction in wireless atm networks,” *Selected Areas in Communications, IEEE Journal on*, vol. 16, no. 6, pp. 922–936, 1998.
- [35] F. T. Pokorny, M. Hawasly, and S. Ramamoorthy, “Multiscale topological trajectory classification with persistent homology,” in *Robotics: Science and Systems X*, 2014.
- [36] F. Pokorny, M. Hawasly, and S. Ramamoorthy, “Topological trajectory classification with filtrations of simplicial complexes and persistent homology,” *International Journal of Robotics Research*, 2015.
- [37] A. Wallar, “Keeper: Using methods of nonlinear regression for position prediction of moving objects.” <https://github.com/wallarelvo/keeper>, 2015.
- [38] A. Wallar, “Racer: Path planning in stochastic dynamic environments in python.” <https://github.com/wallarelvo/racer>, 2015.
- [39] J. D. Hunter, “Matplotlib: A 2d graphics environment,” *Computing In Science & Engineering*, vol. 9, no. 3, pp. 90–95, 2007.
- [40] M. Quigley, K. Conley, B. Gerkey, J. Faust, T. Foote, J. Leibs, R. Wheeler, and A. Y. Ng, “Ros: an open-source robot operating system,” in *ICRA workshop on open source software*, vol. 3, p. 5, 2009.
- [41] A. Wallar, “Dodger: Path planning in stochastic dynamic environments in c++.” <https://github.com/wallarelvo/Dodger>, 2015.
- [42] R. McKee, “Skynet: 5 Things You Didn’t Know.” [http://uk.askmen.com/entertainment/special\\_feature\\_300/339\\_skynet-5-things-you-didnt-know.html](http://uk.askmen.com/entertainment/special_feature_300/339_skynet-5-things-you-didnt-know.html).